



Methods to characterize type, relevance, and interactions of organic matter and microorganisms in fluids along the flow path of a geothermal facility

Alessio Leins^{1,2}, Danaé Bregnard³, Andrea Vieth-Hillebrand¹, Stefanie Poetz¹, Florian Eichinger⁴, Guillaume Cailleau³, Pilar Junier³, and Simona Regenspurg¹

¹GFZ German Research Centre for Geosciences, Telegrafenberg, 14473 Potsdam, Germany

²Institute for Geosciences, Applied Geology, Friedrich Schiller University, Burgweg 11, 07749 Jena, Germany

³Laboratory of Microbiology, Institute of Biology, University of Neuchâtel
Rue Emile-Argand 11, 2000 Neuchâtel, Switzerland

⁴Hydroisotop GmbH, Woelkestraße 9, 85301 Schweitenkirchen, Germany

Correspondence: Alessio Leins (leins@gfz-potsdam.de)

Received: 12 September 2023 – Discussion started: 22 September 2023

Revised: 7 October 2024 – Accepted: 10 October 2024 – Published: 9 December 2024

Abstract. Dissolved organic matter (DOM) and microorganisms were characterized along the flow path of a geothermal facility that produces water from a deep (2800 m) carbonate rock reservoir for energy provision. A variety of analytical techniques were employed to distinguish between natural and synthetic organic matter, determine the composition of the microbial community, and evaluate the role of microorganisms in the operation of the geothermal site in Bad Blumau, Austria. Ion chromatography (IC), liquid chromatography with organic carbon detection (LC-OCD), and Fourier-transform ion cyclotron resonance mass spectrometry (FT-ICR-MS) in negative electrospray ionization (ESI(−)) and positive atmospheric pressure photoionization (APPI(+)) mode were applied to the fluid samples for the purpose of characterizing the composition of DOM and distinguishing natural DOM from a chemical inhibitor used to prevent scaling. The concentrations of dissolved organic carbon (DOC) ranged from 8.5 to 10.4 mg CL^{−1}. The chemical scaling inhibitor contributes approximately 1 mg CL^{−1} of DOC to the produced fluids. Depending on the applied ionization mode, the FT-ICR-MS results show that between 31 % and 65 % of the macromolecular formulas (150–1000 Da) detected in the fluid samples appear to originate from the inhibitor. However, the DOM is primarily composed of low-molecular-weight acids (LMWA), with acetate being the most prevalent, reaching up to 7.4 mg CL^{−1}. To assess

the diversity of the bacterial communities, targeted amplification of the 16S rRNA gene was conducted. The composition of the microbial community exhibited variation along the flow path, with Firmicutes, Proteobacteria, and Thermotogae representing the dominant bacterial phyla. Based on the community composition, metabolic pathways associated with the presence of acetate in the samples were predicted. Microorganisms may produce acetate through diverse fermentation processes, including those involving lysine, pyruvate, and hexitol. Assessing the presence and interaction of organic compounds and microorganisms in geothermal fluids can provide a broader understanding of processes within the geothermal facility. This understanding could be beneficial for efficient operation of a geothermal power plant.

1 Introduction

Deep hydrothermal energy production is becoming increasingly important as an alternative energy source. Geothermal power plants extract heat from subsurface fluids to produce electricity and heat. The depth at which these fluids are extracted can vary from a few hundred meters to a few kilometers. Geothermal power plants face various operational challenges, such as mineral precipitation (scaling) or corrosion of the well casing and the components of the geothermal plant

(Regenspurg et al., 2016; Demir et al., 2014). Scaling and corrosion are caused by hydrochemical reactions related to changes in fluid pressure and temperature during transport or to the presence of metabolic by-products of microorganisms present in fluids (Inagaki et al., 2003; Little and Lee, 2015). Therefore, analyzing the fluids and their composition is crucial for understanding, predicting, and mitigating possible chemical reactions that could compromise the functioning of a geothermal plant. However, the role of organic components has rarely been considered in the analyses performed to characterize geothermal power stations. In recent studies, corrosion and declining injectivity in power plants have been attributed to biofilm formation, microbially induced corrosion (MIC), or microbially induced mineral scaling (Alawi et al., 2011; Vetter, 2012; Lerm et al., 2013; Little and Lee, 2015; Westphal et al., 2019; Brehme et al., 2020; Leins et al., 2022; Madirisha et al., 2022). The growth of these microorganisms may be sustained by organic compounds in the fluids. These compounds can originate from natural sources in the geothermal aquifer or may have been introduced artificially, such as from detergents used during drilling or from the injection of organic scaling inhibitors. Organic acid anions have been reported in various deep subsurface systems, including oil-field waters (Carothers and Kharaka, 1978; Hatton and Hanor, 1984; Kharaka et al., 1985, 1997), waters from fractured crystalline rock (Sherwood Lollar et al., 2021; Kieft et al., 2018), hydrothermal vents (Lang et al., 2010, 2018; McDermott et al., 2015), and fluids from geothermal sites in the Molasse Basin (Alawi et al., 2011; Vetter, 2012; Leins et al., 2022). Their concentrations in fluids can vary by several orders of magnitude, ranging from a few milligrams per liter to 10 000 mg L⁻¹ (Kharaka et al., 1997). The highest concentrations are usually found in oil-field waters and are dominated by acetate followed by propionate, butyrate, and valerate (Carothers and Kharaka, 1978; Fisher and Boles, 1990; Kharaka et al., 1987). In geothermal systems, chemical scaling inhibitors are commonly added to prevent mineral precipitation, thereby ensuring the efficiency of the geothermal facilities. However, the precise composition of these inhibitors is often proprietary and commercially sensitive, leaving the potential impacts on the fluid's chemistry largely unknown. This poses a significant challenge in tracing the relative contribution of the inhibitors within geothermal fluids, particularly in terms of their interactions with dissolved organic carbon (DOC).

To address this challenge, this study focuses on the detailed chemical characterization of both the scaling inhibitor and the geothermal fluids from a power plant located in Bad Blumau, Austria. Given the unknown composition of the inhibitor, a series of analytical techniques were employed to identify its influence on the fluid chemistry. Ion chromatography (IC) was utilized to detect the presence of specific organic acid anions in the fluids and in the scaling inhibitor. However, these organic acid anions represent only a mi-

nor fraction of the detectable DOC in the fluids. In order to comprehensively analyze the DOC, liquid chromatography with organic carbon detection (LC-OCD) was applied to quantify the DOC content and categorize it into its bulk fractions using size exclusion chromatography (SEC). These fractions range from low-molecular-weight acids (LMWA) and neutral compounds (LMWN) to high-molecular-weight compounds like humic substances and biopolymers. Additionally, Fourier-transform ion cyclotron resonance mass spectrometry (FT-ICR-MS) was used to perform a high-resolution analysis of medium- to high-molecular-weight organic compounds within a mass range of 150 to 1000 Da. Since the chemical properties of the inhibitor were unknown, both positive atmospheric pressure photoionization (APPI(+)) and negative electrospray ionization (ESI(-)) modes were used to detect polar and less polar compounds, respectively. FT-ICR-MS provides accurate masses of molecules, enabling the determination of elemental formulas and thus the tracing of the inhibitor's contribution to the geothermal fluids. This approach also helps to identify biomarkers for microorganisms, providing insight into the broader interactions between the inhibitor and the geothermal system on a molecular level.

To the best of our knowledge, this is the first time that FT-ICR-MS has been used to characterize dissolved organic matter (DOM) in fluids from a geothermal power plant. ESI(-) FT-ICR-MS has already been applied to a variety of water systems such as groundwater (McDonough et al., 2020), deep fracture water (Kieft et al., 2018), pore water (D'Andrilli et al., 2010; Rossel et al., 2016; Schmidt et al., 2009), hydrothermal vents (Noowong et al., 2021; Rossel et al., 2017; Gomez-Saez et al., 2016), and marine and terrestrial waters (D'Andrilli et al., 2010; Koch et al., 2008; Minor et al., 2012; Sleighter and Hatcher, 2008).

In addition to the analyses of the DOM, a parallel analysis of bacterial diversity in the fluids was conducted. Targeted amplification of the 16S rRNA gene allowed the assessment of the bacterial diversity present at the same three sampling points. In order to explain the presence of certain organic compounds, we predicted bacterial metabolic pathways based on the known metabolisms of the most dominant microorganisms found in our samples. We evaluated the bacterial metabolic pathways associated with the consumption or production of acetate to determine if changes in the microbial community are associated with changes in the presence of particular organic acids. Changes in the bacterial community and associated metabolic pathways, as well as microbial growth, may impact the efficacy of power plants. Therefore, it is important to assess both the organic compounds and the microbial composition of geothermal fluids.

This study aims to (1) characterize the DOM and microbial community of a deep geothermal fluid using various methods, (2) determine the origin of DOM by distinguishing between natural and synthetic sources, (3) determine the metabolic pathways related to the consumption or production

of acetate, and (4) assess whether the composition of DOM correlates with a change in microbial diversity.

2 Material and methods

2.1 Site description

The geothermal site Bad Blumau is a geothermal power plant and thermal spa located in southeast Austria (upper Styrian Basin as part of the Pannonian Basin). The targeted geothermal system is also utilized by several other spas and types of heat usage in the area. This area was discovered during a hydrocarbon exploration campaign in the second half of the 20th century (Alt-Epping et al., 2013). The Styrian Basin is of Miocene age, composed of Tertiary siliciclastic basin fills that overlie Paleozoic carbonates and phyllites of the Graz Paleozoic, which in turn overlie the crystalline basement (Goldbrunner, 2000; Alt-Epping et al., 2013). The geothermal reservoir in this area is hosted by carbonate rocks, specifically Devonian limestones and dolomites that originated from Paleozoic reef development (Hubmann et al., 2006). The carbonate rocks exhibit good aquifer properties due to intense fracturing caused by tectonic deformation (Goldbrunner, 2000). In addition to its balneological purpose, the site is also used for heat and electricity production, as well as the commercial production of liquefied CO₂ (Alt-Epping et al., 2013). The system operates as a geothermal doublet with an internal distance of 2300 m between the production and injection well, targeting the Paleozoic (Devonian) carbonate at a depth of 2800 m (Goldbrunner, 2000). The reservoir temperature was reported to be 124 °C (Goldbrunner, 2005), while the fluids at the production well head reach 107 °C and are reinjected at approximately 65–50 °C after heat extraction (Westphal et al., 2019). The geothermal fluid rises via natural gas lift of CO₂ at an average flow rate of 20 L s⁻¹. The CO₂ is reported to ascend from the mantle regions along fault zones and is considered a product of the Neogene volcanism of the Styrian Basin (Goldbrunner, 2000). The presence of CO₂ in the system presents a major challenge to the operation of the plant. At a depth of approximately 300–350 m below the surface, CO₂ degassing occurs, resulting in carbonate precipitation (Alt-Epping et al., 2013).

To prevent carbonate scaling, an inhibitor named hydrin 45.3 is injected into the fluid within the production well at a depth of approximately 500 m and at a pressure before CO₂ degassing. The current inhibitor consists of organic polyelectrolytes. However, the exact chemical composition of the inhibitor falls under the protection of commercial and industrial secrecy.

The geothermal fluids at Bad Blumau have been described as NaHCO₃ type with a salinity of approximately 20 g L⁻¹, and a slightly alkaline pH of around 8.0 (Westphal et al., 2019). The CO₂ concentration makes up 99 % of the gases

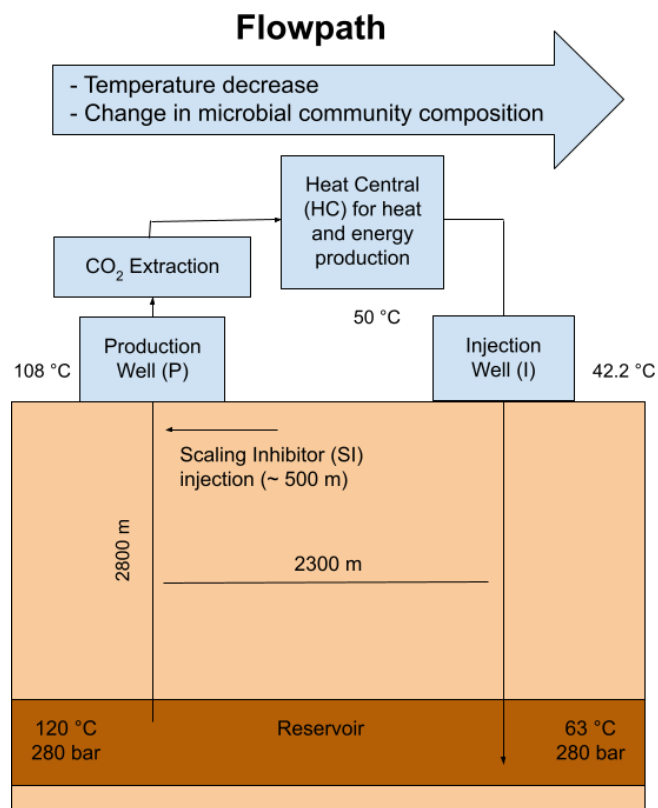


Figure 1. Schematic of the geothermal power plant in Bad Blumau. Modified from Westphal et al. (2019).

and is estimated to be approximately 10 g L⁻¹, which correlates to approximately 5 L of CO₂ per liter of water.

2.2 Sample collection

Fluid samples were collected during two sampling campaigns in March and June 2021. During both campaigns, the geothermal plant was in regular operation. Samples were taken from the surface installations of the plants. The sampling points were at the production well (P) GB2 (*Geothermie Bohrung*, geothermal drilling) before CO₂ extraction, at the heat central (HC), and at the injection well (I) GB1 (Fig. 1). The respective fluids were at approximately 108 °C (P), 50 °C (HC), and 42 °C (I). Unfiltered fluids were collected in 500 mL Duran glass bottles with screw caps containing Teflon-coated septa inside. The bottles were pre-rinsed with the fluid and then completely filled to avoid contact with air. The samples were stored at 4 °C until shipment to the laboratory, where they were stored again at 4 °C until further analyses. In addition to the fluid samples, a sample of the scaling inhibitor used was obtained from the site operators.

For microbial analysis, 40 L of fluid was sampled at each of the three sampling points (P, HC, I) in June 2021. The 40 L of fluids were directly filtered through 0.22 µm nitro-

cellulose membrane filters (Merck Millipore, Germany) under sterile conditions. Filtering of each sample was done using an EZ-Stream pump (Merck Millipore, Germany) and six glass filtration stations mounted on a manifold (Merck Millipore, Germany). This resulted in six filters for each sample that were prepared simultaneously and served as independent replicates. Filters were transported to the laboratory at a temperature of 4 °C and were later stored at –20 °C until further processing.

2.3 Analytical methods

2.3.1 Ion chromatography

The quantification of organic anions (formate, acetate, propionate, butyrate, valerate, oxalate) and inorganic anions (F^- , Cl^- , Br^- , SO_4^{2-}) from both sampling campaigns was performed by IC (ICS 3000, Thermo Fisher Scientific) using an AS-AP autosampler, AS11 high capacity column, and a conductivity detector. KOH solutions with varying concentrations over time were used as an eluent for the samples. The initial KOH concentration was 1.4 mM and gradually increased to 60 mM over a period of 32 min. After 32 min the concentration was reduced to the initial value of 1.4 mM and equilibrated for 12 min. The flow rate was 0.38 mL min^{-1} . The column temperature was 35 °C, and $10 \mu\text{L}$ of the sample was injected for each run. The quality of the measurements was verified daily using standards that contain the analytes in different concentrations. The concentrations were 0.02, 1.0, 10, and 100 mg L^{-1} . For samples with high chloride concentrations ($> 1 \text{ g L}^{-1}$), the chloride was reduced prior to analyzing organic anions using OnGuard II AG/H cartridges (Thermo Fisher Scientific).

2.3.2 Liquid chromatography – organic carbon detection (LC-OCD)

The DOC and its fractions were characterized and quantified using size exclusion chromatography (SEC) with subsequent UV ($\lambda = 254 \text{ nm}$) and IR detection by an LC-OCD system (Huber and Frimmel, 1996) in both sampling campaigns. A mobile phase of phosphate buffer (pH 6.85; $2.7 \text{ g L}^{-1} \text{ KH}_2\text{PO}_4$, $1.6 \text{ g L}^{-1} \text{ Na}_2\text{HPO}_4$) was used, and the flow was adjusted to 1.1 mL min^{-1} (Huber et al., 2011). The samples passed a $0.45 \mu\text{m}$ membrane syringe filter before entering the chromatographic column (Toyopearl HW 50 S; $30 \mu\text{m}$ $250 \text{ mm} \times 20 \text{ mm}$). Here, the DOC was separated into different fractions according to their molecular masses: macro.1 (biopolymers), macro.2 (humic substances), macro.3 (building blocks), low-molecular-weight acids (LMWA), and low-molecular-weight neutrals (LMWN) (Huber et al., 2011). See Table 1 for properties and descriptions of the fractions. DOC was quantified by infrared (IR) detection of the released CO_2 after ultraviolet (UV) oxidation ($\lambda = 185 \text{ nm}$) in a Grätzel thin-film reactor. Humic and fulvic acid standards of the

Suwannee River, provided by the International Humic Substances Society (IHSS), were used for molecular mass calibration. Solutions with known amounts of potassium hydrogen phthalate were used for external calibration of the CO_2 quantification.

2.3.3 Solid-phase extraction (SPE)

Salts are known to cause suppression of ionization (King et al., 2000) and have to be eliminated prior to FT-ICR-MS analysis. Additionally, the concentrations of DOM in natural geothermal water samples are too low for direct analysis by FT-ICR-MS. Therefore, geothermal fluids had to be pre-treated by solid-phase extraction (SPE) on SPE cartridges (PPL Bond Elut 1 g, 6 mL cartridge; Agilent Technologies, Germany) (Dittmar et al., 2008) to obtain salt-free samples and accumulate 1 mg of DOC for the FT-ICR-MS analysis. The sample amount for SPE was adjusted to approximately contain 1 mg of DOC based on the DOC concentration determined by LC-OCD. The fluid samples from March 2021 and the inhibitor sample were filtered using $0.45 \mu\text{m}$ membrane syringe filters, diluted with deionized water (1 : 1) and acidified up to pH 2 with hydrochloric acid (Suprapur) and passed through the cartridges. The cartridges were pre-rinsed with methanol and acidified deionized water (pH 2, hydrochloric acid) to activate the resins. After absorption, the cartridges were rinsed three times with 6 mL of acidified deionized water at pH 2 to remove any remaining salts. The cartridges were dried by vacuum pump for 5 min. Finally, the DOM was eluted with 6 mL of methanol into pre-combusted glass vials, dried in an N_2 atmosphere, and weighed. The dried samples were then stored in the dark at –24 °C until FT-ICR-MS analysis.

2.3.4 Fourier-transform ion cyclotron resonance mass spectrometry (FT-ICR-MS)

FT-ICR-MS, with its ultra-high resolution in combination with atmospheric pressure ionization modes, can provide the elemental composition of thousands of individual medium- to high-molecular weight organic compounds. All DOM samples and the inhibitor were dissolved in methanol (MeOH) to give a stock solution with a final concentration of 1 mg mL^{-1} . The samples were analyzed on a Bruker Solarix FT-ICR-MS with a 12 T refrigerated, actively shielded superconducting magnet. For ESI(–) analysis, the stock solutions were spiked with $4 \mu\text{L}$ of 25 % aqueous ammonia solution. Measurement solutions of $100 \mu\text{g mL}^{-1}$ were prepared in MeOH. Ionization was done with an Apollo II ESI source from Bruker Daltonik GmbH (Bremen, Germany) in negative ion mode. Samples were infused at a flow rate of $150 \mu\text{L h}^{-1}$ using a syringe pump (Hamilton). The capillary voltage was set at 3000 V and an additional collision-induced dissociation (CID) voltage of 70 V was applied at the source to avoid the formation of clusters and adducts. Nitrogen was used as

Table 1. Description of LC-OCD fractions (Zhu et al., 2015). Modified from Huber et al. (2011) and Penru et al. (2013).

Fraction	Molecular mass range	Properties	Description
Hydrophobic organic carbon (HOC)		Hydrophobic	Lipids (fats) released from bacteria and algae, hydrocarbons
Biopolymers (macro.1)	> 10 000 Da	Not UV-absorbable, hydrophilic	Polysaccharides and proteins
Humic substances (macro.2)	~ 1000 Da	Highly UV-absorbable, hydrophobic	Calibration based on Suwannee River standard from IHSS
Building blocks (macro.3)	350–500 Da	UV-absorbable	Breakdown products of humic substances
Low-molecular-weight organic acids (LMWA)	< 350 Da	Negatively charged	Aliphatic acids
Low-molecular-weight neutrals (LMWN)	< 350 Da	Weakly or uncharged hydrophilic, amphiphilic	Alcohols, aldehydes, ketones, amino acids

a drying gas at a flow rate of 4.0 L min^{-1} and a temperature of $220 \text{ }^\circ\text{C}$, and it was used as a nebulizing gas at 1.4 bar. The spectra were recorded in broadband mode using 4 megaword datasets. The ion accumulation time was set at 0.05 s, and 200 scans were collected and added to each mass spectrum. Ions were detected in an m/z range between 150 and 1000.

For the APPI(+) analyses, solutions of $20 \mu\text{g mL}^{-1}$ in MeOH were prepared from the stock solutions. Measurement solutions of $100 \mu\text{g mL}^{-1}$ were prepared in MeOH : *n*-hexane (9 : 1). The ion source used was an APPI-II from Bruker Daltonik GmbH (Bremen, Germany). Samples were introduced into the MS at an infusion flow rate of $20 \mu\text{L min}^{-1}$ using a syringe pump (Hamilton). The capillary voltage was set to -1000 V and CID to 30 V. Nitrogen was used as a drying gas at a flow rate of 3.0 L min^{-1} and a temperature of $210 \text{ }^\circ\text{C}$, as well as being used as a nebulizing gas at 2.3 bar and a temperature of $350 \text{ }^\circ\text{C}$. The spectra were recorded in broadband mode using 4 megaword datasets. The ion accumulation time was set to 0.05 s, and 300 scans were collected and added to each mass spectrum. Ions were detected in an m/z range between 147 and 1500.

In ESI(−), the DOM samples were internally recalibrated using O_x compounds, while for the inhibitor both O_x and S_1O_x compounds were used. In APPI(+), both the fluid samples and the inhibitor sample were internally recalibrated using O_x compounds. The root-mean-square deviations of the eight internal calibrations ranged between 0.013 and 0.018. Method blanks covering sample preparation steps (SPE) and the FT-ICR-MS measurement were prepared for both modes, and blank signals were removed from the DOM signal list of the fluid and the inhibitor samples.

Data evaluation was performed using Data Analysis 4.0 SP5 (Bruker Daltonik GmbH, Germany), Excel 2019 (Microsoft Corporation, Redmond, WA), and the statistical data analysis tool R 4.0.1 (R Core Team, 2020) using the tidyverse package (Wickham et al., 2019). Only m/z values with

a signal-to-noise ratio ≥ 9 were exported for formula assignment. The molecular formulas were calculated considering the isotopes ^{12}C and ^{13}C , with upper elemental thresholds of $\text{O} \leq 32$, $\text{S} \leq 2$, $\text{N} \leq 2$, and unlimited C and H. The mass tolerance was set to $\pm 0.5 \text{ ppm}$, and formulas containing ^{13}C were excluded from the final dataset.

The abundance of inhibitor-derived compounds in the fluids was determined by adding up the total monoisotopic ion abundance (TMIA) of the formulas derived from the inhibitor for each fluid sample.

The double-bond equivalent (DBE) is a measurement to express the number of double bonds and rings. With the respective molecular formula, it can be calculated from the number of carbon (C), hydrogen (H), and nitrogen (N) atoms as follows:

$$\text{DBE} = \text{C} - \frac{\text{H}}{2} + \frac{\text{N}}{2} + 1. \quad (1)$$

Since the DBE counts all double bonds with at least one carbon as a bonding partner, it is not well suited to describe the aromaticity of DOM compounds that contain a high number of double bonds within carboxy groups. Therefore, the DOM-adapted modified aromaticity index (AI_{mod}) described by Koch and Dittmar (2006) has been used, as expressed in Eq. (2), to evaluate the proportion of aromatic compounds in the dataset. It is a measure of the double-bond density in a molecule, taking into account the contribution of heteroatoms. The AI_{mod} is based on the assumption that 50 % of the oxygen is bound with double bonds in carboxyl groups.

$$\text{AI}_{\text{mod}} = \frac{1 + \text{C} - 0.5\text{O} - \text{S} - 0.5(\text{N} + \text{P} + \text{H})}{\text{C} - 0.5\text{O} - \text{N} - \text{S} - \text{P}} \quad (2)$$

Three ranges were established to describe the aromaticity of a given DOM compound. AI_{mod} values ≤ 0.5 are described as aliphatic (Zhu et al., 2019), AI_{mod} between 0.5 and 0.67 represent aromatic compounds, and $\text{AI}_{\text{mod}} \geq 0.67$ describes condensed aromatic compounds (Koch and Dittmar, 2006).

Intensity-weighted averages for DBE; AI_{mod} ; the O/C and H/C ratios; and carbon, hydrogen, and oxygen numbers in each sample were calculated after Bae et al. (2011):

$$\text{var}_{\text{average}} = \frac{\sum_i I_i \cdot (\text{var})_i}{\sum_i I_i}, \quad (3)$$

where I_i and $(\text{var})_i$ are the relative abundances and respective variable values of peak i .

2.3.5 Microbial analysis

Five of the six filters were processed for DNA extraction. The last filter was kept as a backup. DNA extraction was performed with the FastDNA[®] SPIN kit for soil (MP Biomedicals, USA) using three bead-beating rounds and pooling the three independent DNA extracts at the final step (Wunderlin et al., 2013). In parallel, a DNA blank extract was prepared by performing the same procedure without any cellular material. DNA was quantified with the Qubit[®] dsDNA HS Assay Kit and Qubit[®] 2.0 Fluorometer (Invitrogen, Carlsbad, CA, USA). The DNA extracts were sent to FASTERIS SA (Geneva, Switzerland) for amplicon sequencing on an Illumina MiSeq sequencing platform (Illumina, San Diego, CA, USA). The V3–V4 region of the 16S rRNA gene for bacteria was amplified using the Bakt_341F (CCTACGGGNGGCWGCAG) and Bakt_805R (GACTACHVGGGTATCTAATCC) primers (Herlemann et al., 2011). Sequences, provided as pre-trimmed and pre-demultiplexed, were processed with Qiime2 (Bolyen et al., 2019) using the dada2 pipeline (Callahan et al., 2016). Sequences were truncated and joined to full denoised sequences of 464 bp. These sequences were grouped as amplicon sequence variants (ASVs). Taxonomy was assigned using the Silva database, release 132 (Quast et al., 2012), and the vSEARCH-based consensus taxonomy classifier (Rognes et al., 2016). Further analysis was performed in R Studio V3.6.3 using R version 4.2.2 with the phyloseq package (McMurdie and Paulson, 2016), the vegan package (Oksanen et al., 2022), and the ggplot2 package (Wickham, 2016). To represent the metabolic capacities of the community, ASVs corresponding to those found in the DNA blank extract, mitochondria, and chloroplast signals were excluded from the database prior to exporting the representative sequences and the ASV count table. A taxonomy was then assigned to the PYCRUST2 (Douglas et al., 2020) pipeline outputs using the SILVA database (Quast et al., 2012) to highlight organisms' involvement in metabolic functionalities, such as those related to acetate production or degradation. These steps were performed in R using the biomformat (McMurdie and Paulson, 2016), tidyverse (Wickham et al., 2019), and ggplot2 (Wickham, 2016) packages.

3 Results

3.1 Organic and inorganic anions

IC analyses show relatively constant concentrations of Cl^- and F^- throughout the power plant, with around 4 g L^{-1} and 10 mg L^{-1} , respectively (Table 2). The SO_4^{2-} values ranged from 500 to 570 mg L^{-1} . Bromide concentrations ranged from 2.6 to 15.2 mg L^{-1} . Cl^- and SO_4^{2-} were slightly lower, with around 3.4 g L^{-1} and 490 mg L^{-1} , respectively, compared to Westphal et al. (2019). Acetate was the predominant organic acid anion, with concentrations ranging from 5.8 to 7.4 mg CL^{-1} . Propionate was found slightly above the detection limit, with 0.6 mg CL^{-1} in the injection side sample from June. Formate, butyrate, valerate, and oxalate were not detected ($< 0.6 \text{ mg CL}^{-1}$). The inhibitor analyses showed 220 mg CL^{-1} of acetate, suggesting that with the reported addition of 10 mg L^{-1} of inhibitor to the fluids, $2.2 \mu\text{g CL}^{-1}$ acetate could have been added from the inhibitor.

3.2 DOC and bulk fractions

The DOC in the fluid samples ranged from 8.5 to 10.4 mg CL^{-1} (Table 2). In March, the DOC decreased from the production to the injection side, whereas in June the concentrations were quite similar in the production and injection sides and slightly higher at the heat central. According to Westphal et al. (2019), the concentration of DOC was found to be 14.5 mg CL^{-1} in the production sample and 4 mg CL^{-1} in the injection sample. A decrease in DOC concentration was observed along the pathway. However, a stronger one compared to this study. The inhibitor DOC comprises 102 g CL^{-1} . With the reported dosage, the inhibitor contributes approximately 1 mg CL^{-1} to the total DOC of the fluids. The DOC fractions measured by size exclusion chromatography show a predominant LMWA fraction in all samples (Table 2), which is likely due to the high acetate concentrations in the fluid. The macro fraction is the second-most abundant (16%–19%), followed by the LMWN fraction (8%–12%). In this study, we were unable to distinguish between the macro.1, macro.2, and macro.3 fractions, since the chromatograms display only one peak spanning across the retention times for all three macro fractions. Therefore, this peak represents the whole macro fraction (10 000–350 Da). Hydrophobic organic carbon (HOC) was detected only in the March samples (13%–19%). The relative abundance of the LMWA fraction along the flow path in both campaigns correlates with the respective organic acid anion trends of the samples. In the inhibitor sample, the macro fraction represents 99% of the DOC. By utilizing the macro fraction provided by the SEC in the fluid samples and the inhibitor dosage, we determined that approximately 60%–74% of the macro fraction in the fluid samples originates from the inhibitor.

Table 2. DOC, concentrations of organic and inorganic anions, and relative abundance of the DOC fractions in the production (P), heat central (HC), injection (I) fluid, and inhibitor (SI) samples for the sampling campaign in March 2021 and June 2021 measured by LC-OCD and IC. Fluid data were compiled from Leins et al. (2023).

	March 2021			June 2021			SI
	P	HC	I	P	HC	I	
Cl ⁻ (g L ⁻¹)	3.9	4.1	4.0	4.0	3.9	3.7	0.14
SO ₄ ²⁻ (mg L ⁻¹)	544	570	554	545	520	500	14.7
F ⁻ (mg L ⁻¹)	10.1	10.3	10.2	10.5	10.6	10.4	2
Br ⁻ (mg L ⁻¹)	2.7	2.6	4.5	12.4	12.2	15.2	< 1
Acetate							
(mg L ⁻¹)	17.2	16.7	14.2	17.9	18.2	17.9	542
(mg CL ⁻¹)	7	6.8	5.8	7.3	7.4	7.3	220
Propionate							
(mg L ⁻¹)	< 1	< 1	< 1	< 1	< 1	1.3	< 1
(mg CL ⁻¹)						0.6	
Σ organic acid anions							
(mg L ⁻¹)	17.2	16.7	14.2	17.9	19.5	19.1	542
(mg CL ⁻¹)	7	6.8	5.7	7.3	7.4	7.9	220
DOC (mg C L ⁻¹)	10.4	10	8.6	8.8	9.2	8.5	102 180
DOC fractions							
HOC %	13	13	19	0	0	0	0
Macro %	16	17	19	17	17	19	99
LMWA %	59	61	54	72	72	72	0
LMWN %	12	9	8	11	11	9	1

3.3 Molecular composition of the DOM

While LC-OCD analyses provide general information about the molecular size distribution of the DOM, FT-ICR-MS enables highly resolved insight into the molecular composition of DOM compounds within a mass range from approximately 150 to 1000 Da. Acidic compounds are detected in ESI(-), and low-polarity neutral compounds are characterized using APPI(+) mode.

3.3.1 ESI(-) FT-ICR-MS

Inhibitor sample

Negative mode ESI FT-ICR-MS of the Bad Blumau samples provided several hundred assigned formulas in the mass-to-charge (m/z) range of 157–987 (Table 3). The main compound classes in the DOM of the inhibitor sample were, in decreasing abundance, O_x, accounting for 73 % TMIA; S₁O_x, with 22 % TMIA; N₁S₁O_x, with 2.9 % TMIA; and N₁O_x, with 2 % TMIA (Fig. 2). A total of 472 formulas were assigned to the inhibitor sample, with an average atom number of 22.7 for carbon (C), 29.9 for hydrogen (H), and 15.2 for oxygen (O). The number-averaged molecular weight

(M_n) and weight-averaged molecular weight (M_w) were calculated as 554.9 and 670.7, respectively. The average DBE was calculated as 8.33, and the AI_{mod} with a value of 0.08 indicates that the majority of the signals consist of aliphatic compounds (AI_{mod} ≤ 0.5) (Table 3).

The O_x class exhibits an increasing relative abundance of compounds within the O_{1–8} range (Fig. 3). In the O_{10–30} range, the even-numbered compounds display significantly higher relative abundances compared to their odd-numbered counterparts. The N₁O_x compounds, although few, are predominantly present as odd-numbered oxygen compounds within the N₁O_{5–15} range. Similarly, the S₁O_x compounds are mainly observed as odd-numbered oxygen compounds, particularly within the S₁O_{13–27} range. Lastly, the N₁S₁O_x compounds are characterized by lower oxygen counts, with a notable presence of even-numbered oxygen compounds in the N₁S₁O_{8–20} range.

Fluid samples

The main compound classes in the DOM of the fluid samples show a similar distribution to the inhibitor sample, with oxygen-containing compounds (O_x) with around 67 % of the TMIA, sulfur- and oxygen-containing compounds (S₁O_x)

with 23 %TMIA–27 %TMIA, and nitrogen-, sulfur-, and oxygen-containing compounds ($N_1S_1O_x$) with 4.5 %TMIA–4.7 %TMIA. N_1O_x compounds were found only in the production side sample (0.4 %TMIA). In direct comparison, 31 %–65 % of the TMIA in the fluid samples derives from formulas that are also present in the inhibitor samples. The abundance of inhibitor-derived compounds decreases from the production side (65 %TMIA) to the heat central (31 %TMIA), followed by an increase to the injection side (42 %TMIA) (Table 3).

The sample with the highest number of formulae assigned is the heat central (Table 3). The mean number of atoms in the fluid samples range from 22.9 to 24.2 (C), 29.3 to 31.9 (H), and 15.9 to 16.8 (O). The M_n and M_w range from 569.3 to 595 and 623.3 to 639.9, respectively, and DBE values are around 8.5–8.9 (Table 3). The AI_{mod} range from 0.04 to 0.05 indicates that the majority of the signals consist of aliphatic compounds ($AI_{mod} \leq 0.5$).

The O_x class ($x = 1–32$) exhibits a roughly Gaussian distribution of relative abundances, with a dominant presence in the $O_{12–24}$ range (P, HC, I) (Fig. 3). Notably, the even-numbered compounds within this range display a significantly higher relative abundance. The S_1O_x compounds are primarily composed of odd numbers of oxygen atoms, ranging from S_1O_{13} to S_1O_{27} , and show a higher relative abundance compared to other S_1O_x signals. These distinct peaks in both the $O_{12–24}$ and $S_1O_{13–27}$ compounds align with the dominant peaks observed in the inhibitor sample. The few N_1O_x compounds also exhibit odd oxygen numbers, similar to those found in the inhibitor, indicating that these compounds were clearly introduced by the inhibitor. However, they were only detected in the production side sample. In contrast, the $N_1S_1O_x$ compounds appear to be less affected by the inhibitor, with $N_1S_1O_4$ and likely the even-numbered oxygen compounds within the range of $N_1S_1O_{8–20}$ being introduced by the inhibitor.

3.3.2 APPI(+) FT-ICR-MS

Inhibitor sample

APPI FT-ICR-MS of the Bad Blumau fluid samples provided assigned formulas in the m/z range of 193–1019 (Table 3). A total of 1741 formulas were assigned to the inhibitor sample. The predominant compound classes in the DOM were O_x , comprising 82 %TMIA, followed by S_1O_x at 9.3 %TMIA. $N_1S_1O_x$ compounds made up 4.7 %TMIA, while N_1O_x compounds had the lowest abundance at 1.3 %TMIA. (Fig. 2). The average number of atoms in the inhibitor sample is 22.7 (C), 28.8 (H), and 12.8 (O), with a mean (DBE) value of 8.78 (Table 3). The average AI_{mod} of 0.16 indicates that the inhibitor compounds are primarily aliphatic. The number-averaged molecular weight (M_n) and weight-averaged molecular weight (M_w) are 511.9 and 543.2, respectively.

The distribution of O_x compounds in the fluid samples follows a Gaussian pattern centered around O_{13} (Fig. 3). In contrast, only small amounts of S_1O_x , N_1O_x , and $N_1S_1O_x$ compounds with no specific distribution patterns were observed in the inhibitor sample.

Fluid samples

The main compound classes in the DOM of the fluid samples were, in order of predominance, O_x , with 69 %TMIA–76 %TMIA; S_1O_x , with 6 %TMIA–9.2 %TMIA; and N_1O_x , with 2.8 %TMIA–3.5 %TMIA. Up to 64 % of the TMIA in the fluid samples originate from formulas that are also present in the inhibitor sample. The abundance decreases from the production side (64 %TMIA) to the injection side (58 %TMIA). The mean number of atoms in the fluid samples ranges from 20.8 to 21.2 (C), 24.5 to 25.8 (H), and 9.5 to 10 (O). Notably, the mean oxygen numbers decrease from the production side to the injection side (10 to 9.52) and are lower than the mean oxygen number observed in the inhibitor sample (12.8). The DBE values range from 9 to 9.8, and the AI_{mod} of approximately 0.23 indicates that the compounds are primarily aliphatic. (Table 3). The M_n and M_w range from 433.8 to 440.6 and 461.3 to 473.6, respectively. The O_x class in the fluid samples shows a Gaussian distribution centered around $O_{9–12}$ (Fig. 3). Similarly to the inhibitor, only small amounts of S_1O_x and N_1O_x compounds were detected in the fluid samples, with no specific distribution pattern observed. Additionally, $N_1S_1O_x$ compounds were unique to the inhibitor and were not found in the fluid samples. A comparison of the assigned O_x signals in the fluids with those in the inhibitor reveals that the inhibitor introduces a substantial amount, accounting for up to 63.2 % of the signals present in the fluids.

3.4 Microorganisms in the fluids

The composition of the bacterial communities in the fluids was investigated by amplicon sequencing of the 16S rRNA gene. The relative abundance of the 10 most abundant bacterial phyla present in the three sampling sides is shown in Fig. 4. A very significant shift in community composition was consistently detected in the replicate samples of the three sampling points. In all three, the Firmicutes phylum was dominant. Amplicon sequence variants (ASVs) assigned to Proteobacteria were present in a small relative abundance in the production well but became highly abundant (co-dominant with ASVs from Firmicutes) in the heat central. However, on the injection side, Proteobacteria were not detected and were replaced by the *Thermotogae* phylum, which dominated the community together with Firmicutes. The *Thermotogae* phylum was also detected in all replicates from the heat central but at a much lower relative abundance. In addition to the dominant phyla, there was also a low abundance of *Actinobacteria*, *Cyanobacte-*

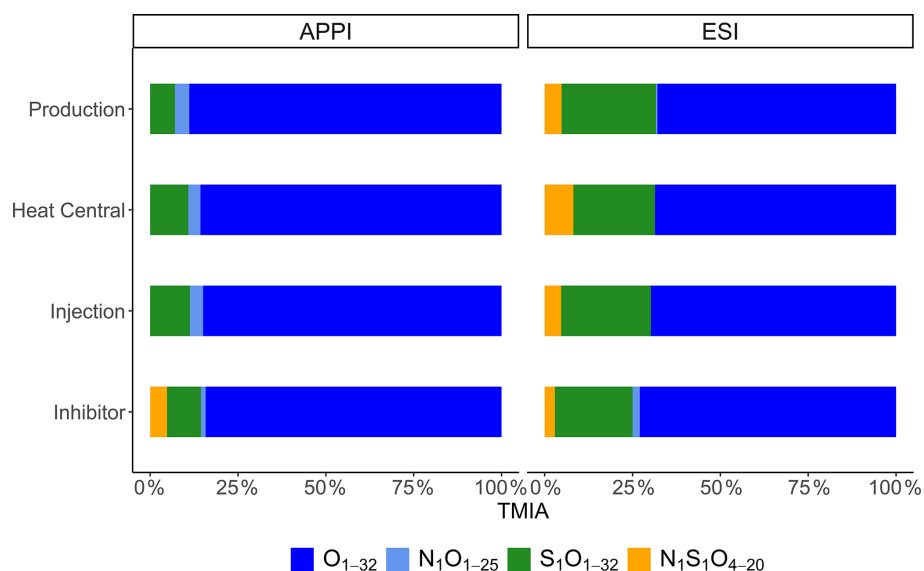


Figure 2. Relative abundances of assigned compound classes (O_x , N_1O_x , S_1O_x , and $N_1S_1O_x$) in APPI and ESI modes.

Table 3. Total and unique numbers of assigned monoisotopic signals within their sample group, including the distribution of the main elemental classes, total mass range, percentage of TMIA derived from inhibitor signals, intensity-weighted averages of the elemental numbers (carbon, hydrogen, oxygen), DBE, AI_{mod} , and molecular weight.

Well	No. of formulas					Mass range (Da)	SI amount (TMIA %)	Mean					M_n Total	M_w Total	
	Total	O_x	N_1O_x	S_1O_x	$N_1S_1O_x$			Unique	C	H	O	DBE			AI_{mod}
ESI negative															
P	669	521	5	80	63	106	171–995	65 (280)	23	29.3	16.8	8.93	0.04	582.1	629.6
HC	809	619	0	82	108	198	179–981	31 (241)	24.2	31.9	16.4	8.75	0.04	595	639.9
I	573	469	0	61	43	16	165–987	42 (222)	22.9	29.8	15.9	8.47	0.05	569.3	623.3
SI	472	409	7	40	16	148	157–987	–	22.7	29.9	15.2	8.33	0.08	554.9	670.7
APPI positive															
P	700	594	55	51	0	46	209–1019	64 (496)	20.8	24.5	10	9.05	0.22	436.6	467.6
HC	649	547	39	63	0	52	193–1019	58 (460)	21.2	25.8	9.74	9.85	0.23	440.6	473.6
I	649	555	43	50	0	40	209–912	58 (463)	21	25	9.52	9.05	0.24	433.8	461.3
SI	1741	1276	82	189	194	1262	181–1175	–	22.7	28.8	12.8	8.78	0.16	511.9	543.2

M_n – number-averaged molecular weight. M_w – weight-averaged molecular weight.

ria, and *Planctomycetes*, followed by a few *Nitrospirae* (in one sample), *Thermotogae* (in one sample), and *Verrucomicrobia* in the production side. Low abundances of *Thermotogae*, *Actinobacteria*, and *Nitrospirae* were observed in the heat central, and low abundance of *Thermotogae*, as well as an extremely low relative abundances of *Actinobacteria* and *Bacteroidetes*, were observed on the injection side. The same analysis was performed at a lower taxonomic rank. At the genus level, drastic changes in the composition of the bacterial community at different sampling points were more clearly observed. The relative abundance of the 10 most abundant genera per sampling point is represented in Fig. 5. The genus *Bacillus* (Firmicutes) dominated the fluids in the production well. *Caulobacter* (Proteobacteria) and SCADC1-2-3 (Firmicutes) were dominant

in the heat central, while the sulfate-reducing bacteria (SRB) *Desulfotomaculum* (Firmicutes) was dominant on the injection side. The top five genera represent around 60 % of the detected community in the production well and the heat central, while the top five genera represent around 75 % of the community on the injection side. This suggests that the community on the injection side was less diverse than the communities present on the other two sides. The metabolic potential of the bacterial communities in Bad Blumau was assessed based on the phylogenetic composition using PICRUSt2 (Douglas et al., 2020). It predicts the metabolic capacities of a given bacterial genus based on the conserved V3–V4 regions of the bacterial 16S rRNA gene. After predicting the pathways that may be present, the software also estimates the contribution of bacteria from a given

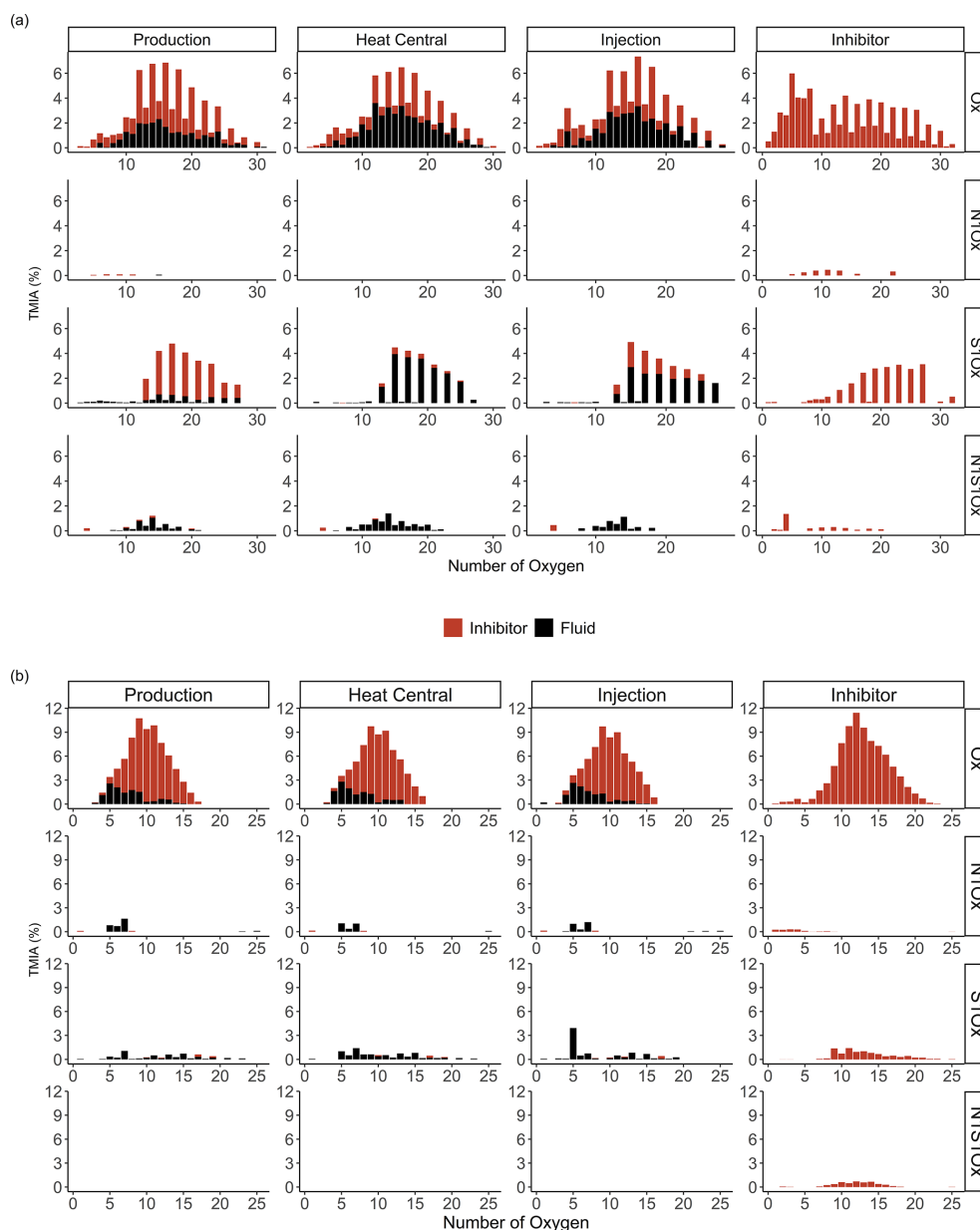


Figure 3. TMA vs. number of oxygen molecules for every compound class and sample in (a) APPI(+) and (b) ESI(−) mode. Data colored red within the fluid samples represent the fluid signals that correspond to the signals found in the inhibitor sample.

genus to the predicted pathway. The potential metabolisms that resulted in the production of acetate were the fermentation of lysine to acetate and butyrate; the fermentation of pyruvate to acetate and lactate; and the fermentation of hexitol, which can also lead to the production of lactate, formate, ethanol, and acetate (Fig. 6). Acetate can then be used in methanogenesis (Fig. 6). *Bacillus* was the dominant genus that contributed to the identified metabolic pathways on the production side, while *Desulfotomaculum* was the dominant genus on the injection side. The heat central, depending on the targeted metabolism, represented a transition between the production and injection points or was dominated by a dif-

ferent genus, such as the *Caulobacter* genus in the case of lysine fermentation (Fig. 6).

4 Discussion

LC-OCD analyses provided a good general overview of the DOC fractions in the geothermal fluids, showing that most of the DOM is present in the LMWA fraction. IC results confirmed that this acid fraction is mainly composed of acetate. Using FT-ICR-MS, we successfully analyzed the molecular formulas of the macromolecular inventory and characterized

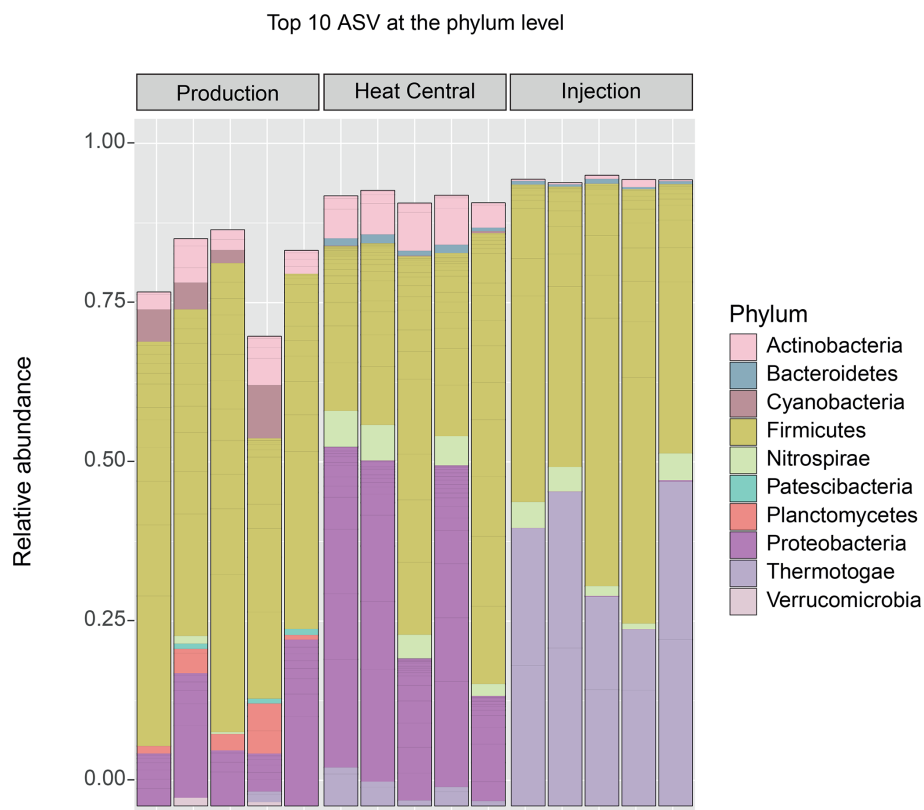


Figure 4. Top 10 bacterial phyla by relative abundance (in all samples). The ASVs not assigned to any phylum (unclassified) are not shown.

the organic compounds present in the fluids derived from the inhibitor. This raises the following questions. (1) Is it possible to characterize and subtract synthetic organic matter to obtain an indication of the natural organic matter in geothermal fluids? (2) Why do DOM and microbial diversity change along the fluid pathway, and is there a correlation between the two? (3) Where does the acetate derive from, and what is the metabolic pathway for it? These three questions are discussed below.

4.1 DOM composition and impact of the inhibitor in the fluid of the deep geothermal site Bad Blumau

The overall decrease in abundance of inhibitor-derived signals from the production to the injection side in ESI(–) mode could be an indication of degradation, alteration, or dilution of the inhibitor along the fluid pathway. The strong overlap between odd-numbered S_1O_{13-27} compounds in the fluid and inhibitor samples suggests that these compounds derive mainly from the inhibitor (Fig. 3). The assigned signals from the fluid and inhibitor samples indicate a strong influence of the inhibitor on the production side sample, with contributions reaching up to 65%. Both the heat central and injection side samples do not show such a strong overlap with the inhibitor sample. However, it is likely that these S_1O_x compounds have undergone chemical alteration along the flow

path and are therefore no longer detectable in the fluid samples from the heat central and injection side. A similar result can be seen for the O_x compound class after subtracting the inhibitor signals. Another strong influence of the inhibitor can be observed on the intensity-weighted average of the molecular O/C ratio on the production side (Table 4). The O/C ratio is higher with inhibitor components and could be explained by the S_1O_{13-27} , which was mainly identical to inhibitor signals in the production side but not in the heat central and on the injection side.

Van Krevelen diagrams were used to visualize compositional differences in the samples by presenting the molecular ratio of H/C and O/C atoms. To simplify the comparison, we followed the differentiation into four groups with different H/C and O/C ranges after Zhu et al. (2019) (I – H/C > 1 and O/C < 0.5 including lipids, proteins, and part of the lignins; II – H/C > 1 and O/C > 0.5 including amino sugars, carbohydrates, and part of the tannins; III – H/C < 1 and O/C < 0.5 including condensed hydrocarbons and part of the lignins; and IV – H/C < 1 and O/C > 0.5 including partially condensed hydrocarbons and tannins). Most of the signals in the fluid and inhibitor samples of the ESI data are present in area II (Fig. 7). Approximately half of the signals from the fluid samples that are plotted in area II of the van Krevelen diagram are consistent with the inhibitor signals. In area I, the fluid samples from the heat central and injection

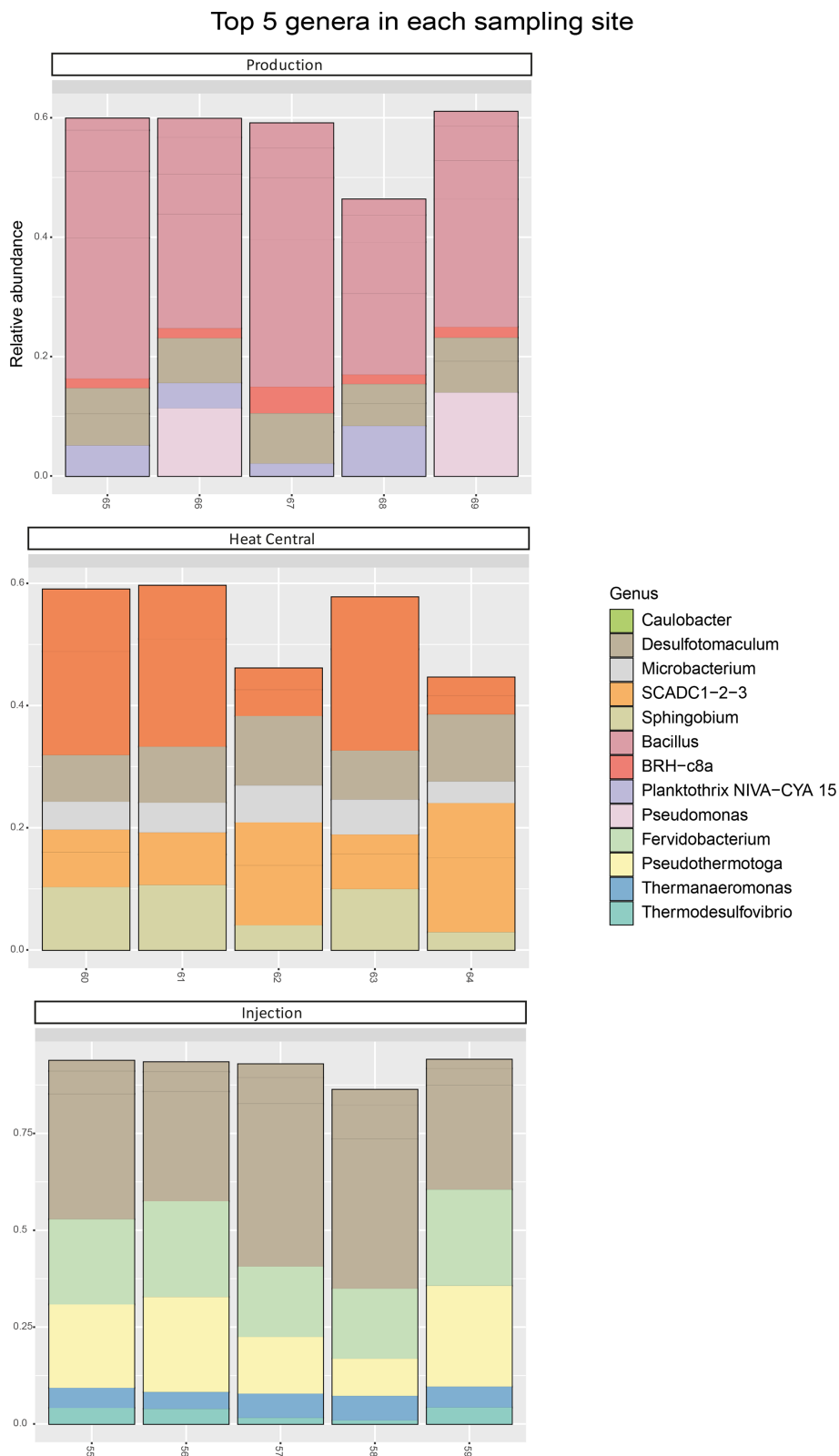


Figure 5. Top five bacterial genera by relative abundance (calculated for each sampling point separately). The ASVs not assigned to any phylum (unclassified) are not shown.

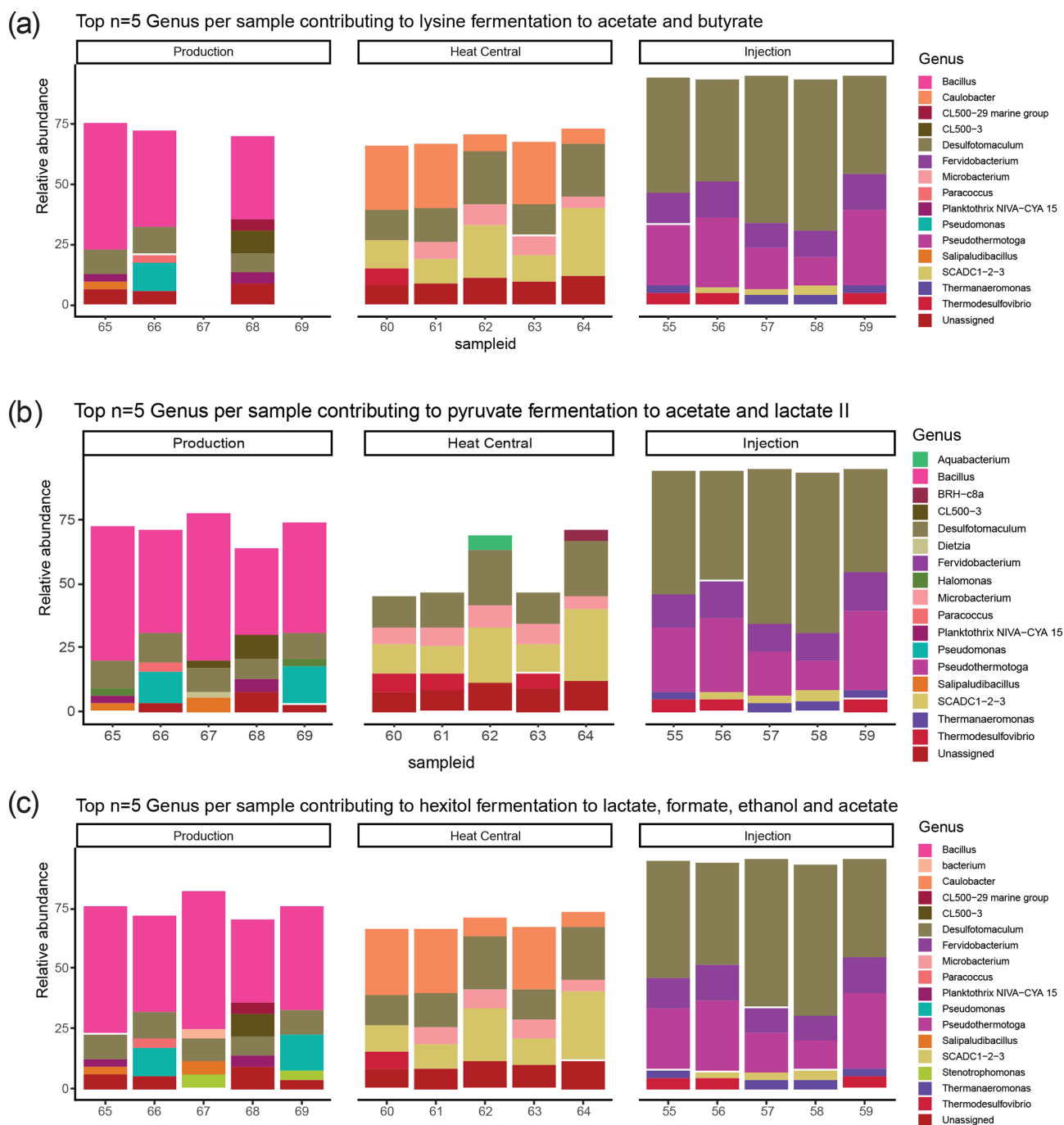


Figure 6. Top five genera per sample and their relative abundance in **(a)** lysine to acetate and butyrate fermentation; **(b)** pyruvate fermentation to acetate and lactate II; **(c)** hexitol fermentation to lactate, formate, ethanol, and acetate; and **(d)** methanogenesis from acetate. Sample ID (55–69) on the *x* axis represents the numbers assigned to each filter.

side mainly show inhibitor-derived formulas with lower H/C (< 1.6) values (Fig. 8).

Similar to the ESI(–) dataset, the APPI(+) data show that the proportion of the TMIA in the fluid samples derived from the inhibitor decreases from the production side to the injection side. The inhibitor affects especially the O_x class

(Fig. 3). Removing inhibitor signals results in a shift in the O_x distribution from O_{9-12} to O_{3-9} , centered around O_5 in the fluid samples. O_x compounds with more than 15 oxygen atoms are found exclusively in the inhibitor (Fig. 3). The introduction of molecules with high numbers of oxygen is also

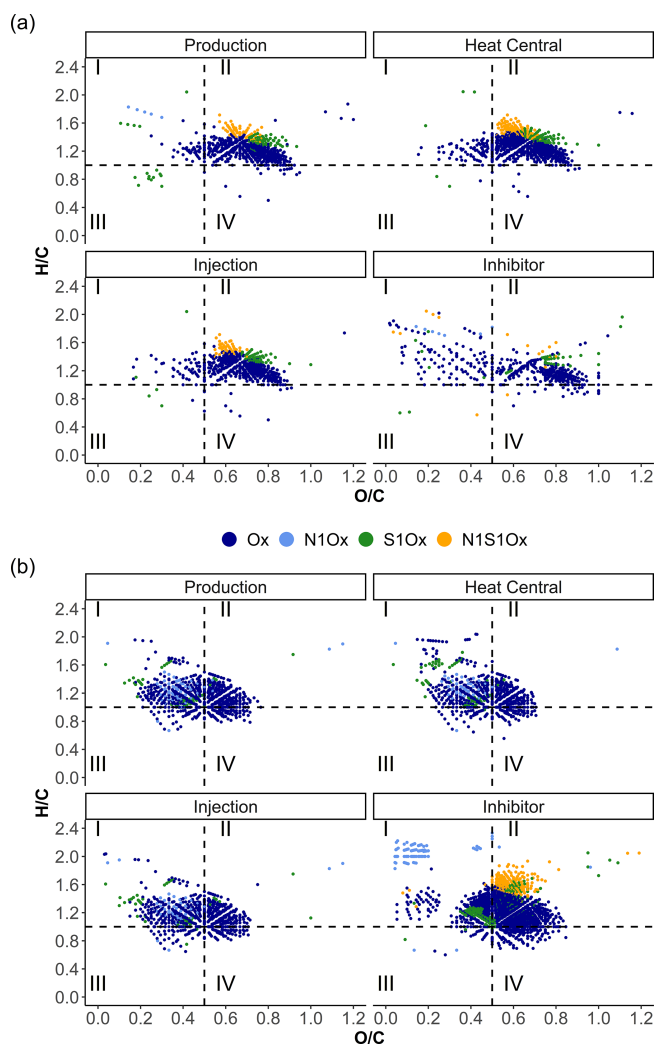


Figure 7. Van Krevelen diagrams of the fluid and inhibitor samples in (a) ESI(–) and (b) APPI(+) modes color-coded by the assigned compound classes.

shown by the decrease in the average O/C ratios if inhibitor signals are removed from the data (Table 4).

The APPI data show distinct patterns for the fluid and inhibitor samples in the van Krevelen diagrams (Fig. 8). Most of the signals in the fluid samples accumulate in area I, while the inhibitor sample shows a strong accumulation in area II and a weaker accumulation in area I at O/C < 0.2. Signals that were only found in the fluid samples are mainly present in the O/C and H/C ranges of 0.2–0.4 and 1–1.7, respectively. They represent the O_x as well as the distinct N_1O_x and S_1O_x compound classes compared to the inhibitor compounds. Typically, signals in this range are attributed to compounds derived from proteins (Sleighter and Hatcher, 2007). These signals may represent microbial activity, since microorganisms have been reported in Bad Blumau fluids (Westphal et al., 2019). Generally, signals within the lipid group of the van Krevelen diagrams (H/C around 2 and O/C

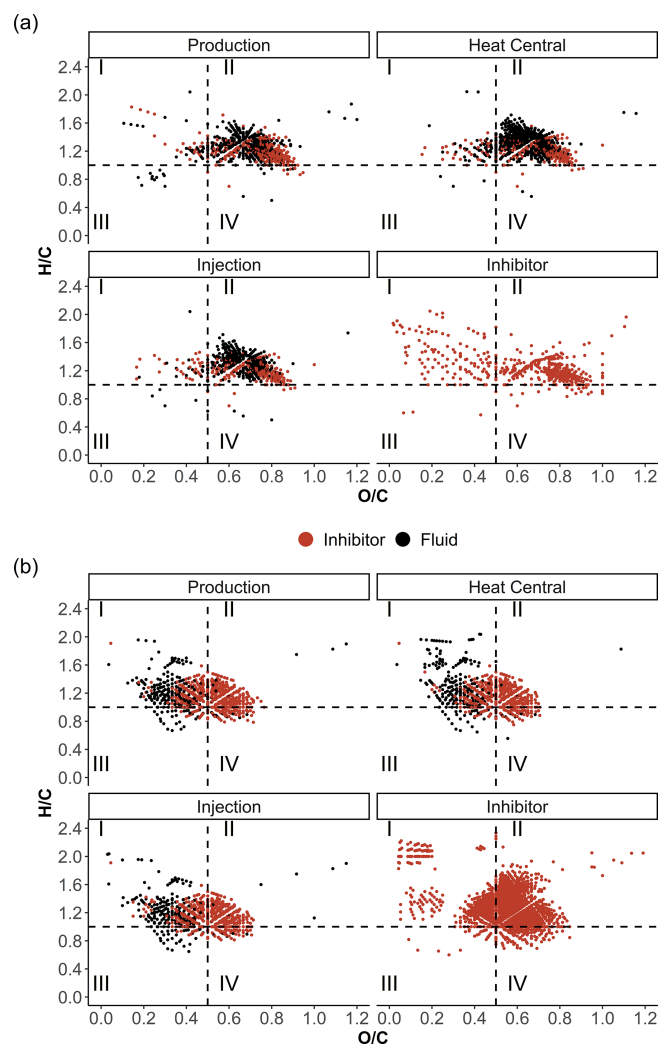


Figure 8. Van Krevelen diagrams of the fluid and inhibitor samples in (a) ESI(–) and (b) APPI(+) modes color-coded by matching signals in the inhibitor and fluid samples.

below 0.2) represent compounds deriving from cell membranes of microorganisms (Sleighter and Hatcher, 2007) and therefore are also good indicators of microbial activity. In particular, the heat central sample shows an accumulation of signals in this area. According to Westphal et al. (2019), microorganisms in the Bad Blumau fluids were likely to feed on the macromolecular organic matter introduced by the scaling inhibitor. FT-ICR-MS data show certain compound classes that are present in the inhibitor sample but absent in the fluid samples (Fig. 4). This is observed in the APPI(+) N_1O_x , S_1O_x , and $N_1S_1O_x$ as well as ESI(–) N_1O_x , and $N_1S_1O_x$ compound classes. The absence of these inhibitor-specific compounds in the fluid samples could be explained by (1) alteration in the form of chemical reactions with the fluid-forming complexes, (2) degradation after the injection into the fluids, (3) no detection in the fluid samples due to strong

dilution of the inhibitor, and (4) degradation by microorganisms that target these specific compounds.

The major absence of signals in areas III and IV of the van Krevelen diagrams in both ionization modes suggests low amounts of highly condensed and aromatic compounds (Kim et al., 2003; Sleighter and Hatcher, 2007). A wider range of signals with H/C ratios below 1 were observed in deep groundwater DOM (McDonough et al., 2022). A strongly different distribution of DOM signals was reported for coal water extracts (kerogen type III), where the majority of the signals were found at H/C ratios below 1 in areas III and IV (Zhu et al., 2019).

Both ionization modes show only a few aromatic compounds derived from the inhibitor. However, those deriving from the inhibitor have a notable effect on the TMIA in the APPI(+) dataset, since the aromatic abundance decreases in the inhibitor-filtered data (Table 4). Aromatic and condensed aromatic compounds may be of natural origin from the reservoir or from other sources. For example, aromatic S_1O_x compounds detected by ESI(−) mode in the fluid samples could be polystyrene-, naphthalene-, and lignosulfates, which are used as super-plasticizers in cement (Flatt and Schober, 2012; Hewlett et al., 2019) and could derive from the casing of the borehole. These data suggest the absence or only a very low impact of petroleum hydrocarbons on the fluids since only a low proportion of DOM signals are present in areas III and IV. A complete lack of signals was observed in areas III and IV in the deep fracture water DOM of the Witwatersrand Basin, which was explained by the low contribution of hydrocarbons from the organic-rich reefs of the Witwatersrand Supergroup (Kieft et al., 2018).

A major difference in the intensity-weighted average O/C values is shown when the Bad Blumau fluid samples are compared to other natural DOM detected by ESI(−) mode. The Bad Blumau samples exhibit high average O/C and H/C values, from 0.65 to 0.68 and 1.26 to 1.33, respectively. The average values for marine, pore, and river waters were reported in the O/C and H/C ranges of 0.32 to 0.52 and 1.13 to 1.29, respectively (Koch et al., 2008; Sleighter and Hatcher, 2008). Studies investigating the DOM of hydrothermal fluids reported average O/C values of 0.25 to 0.35 and generally high H/C ratios above 1.35 (Noowong et al., 2021; Gomez-Saez et al., 2016). Higher O/C values are generally attributed to tannine-like compounds in areas II and IV at O/C greater than 0.5 and H/C around 1 (Sleighter and Hatcher, 2007), originating from terrestrial plant matter and some algae (De Leeuw and Largeau, 1993). However, compound types deriving from algal detritus and/or microbial biomass in marine sediments are reflected by lower O/C and higher H/C ratios (Sleighter and Hatcher, 2008), which is shown in our APPI(+) data but not in the ESI(−) results. A contribution from higher plants is unlikely, since the Bad Blumau reservoir rock was formed during Paleozoic reef development. However, data on deuterium and oxygen isotopes indicate an influence of meteoric water for the

deep thermal Bad Blumau fluids (Goldbrunner, 2000). The higher O/C ratios in the ESI(−) data could be the result of terrestrial DOM being transported into the subsurface. However, within a geothermal setting, the DOM is likely to undergo thermal degradation. Elevated temperature experiments with marine DOM showed a preferential loss of high-molecular-weight and oxygen-rich molecules within 2 weeks of run time (Hawkes et al., 2016). The experiments were conducted in the temperature range of 100–380 °C and suggested that abiotic hydrothermal alteration may start at temperatures above 68 °C. It is unlikely that at the Bad Blumau reservoir temperatures of 124 °C, the intensity-weighted average O/C ratios calculated for the ESI(−) formulas, would show such high values for the DOM originating from reservoir fluids. Another explanation for the still high O/C ratios could be the strong influence of artificial DOM, even after filtering all signals deriving from the inhibitor. Contrary to the ESI(−) data, the inhibitor-filtered APPI(+) data show average O/C and H/C values from 0.33 to 0.35 and 1.23 to 1.3, respectively, which are in good agreement with the hydrothermal vent DOM detected by ESI(−) mode (Noowong et al., 2021; Gomez-Saez et al., 2016). The average DBE values of both APPI(+) and ESI(−) measurements are generally in the same range as diffuse hydrothermal fluid DOM with temperatures up to 170 °C (Noowong et al., 2021; Gomez-Saez et al., 2016). Hotter fluids (> 300 °C) were reported with much higher average DBE values. The low grade of aromaticity in the Bad Blumau DOM with average AI_{mod} values below 0.25 coincides with the hydrothermal vent and thermally altered marine DOM (Noowong et al., 2021; Gomez-Saez et al., 2016; Hawkes et al., 2016). It was stated that elevated temperatures under hydrothermal conditions likely resulted in a decrease in molecular formulas detected by FT-ICR-MS due to a loss of thermally unstable DOM (Noowong et al., 2021; Hawkes et al., 2016; Rossel et al., 2017; Longnecker et al., 2018). This assumption could explain the relatively low number of formulas in the Bad Blumau fluid DOM (< 10³), as a similar range of detected formulas was reported for the hydrothermal DOM (Noowong et al., 2021).

Answering the first question posed for the discussion, we were able to characterize the major parts of synthetic DOM in the fluid and present a DOM fingerprint that better reflects the natural composition of the Bad Blumau geothermal fluids.

4.2 Variation in the composition of DOM and microbial community along the flow path

The DOM composition does not show much variation along the flow path. Most notable are the signals in area I and III of the production side sample at H/C 1.7 and 0.8 in ESI(−) mode and the cluster in area I of the heat central at H/C 1.7 in APPI(+) mode (Fig. 8). The ESI(−) signals are either N_1O_x or S_1O_x that derive from the inhibitor or from other artificial sources. The distinct APPI(+) signals in the heat central derived solely from the inhibitor. It is important to note that

Table 4. Comparison of the average and standard deviations of intensity-weighted averages of DBE, AI_{mod} , and the H/C and O/C ratios of all detected APPI(+) and ESI(−) signals and signals when the inhibitor was removed from the dataset (w/o Inh.). The proportion of aromatic compounds is given as %TMIA.

	ESI						APPI					
	Production		Heat central		Injection		Production		Heat central		Injection	
	All	w/o Inh.	All	w/o Inh.	All	w/o Inh.	All	w/o Inh.	All	w/o Inh.	All	w/o Inh.
H/C ratio	1.26	1.29	1.31	1.36	1.29	1.33	1.17	1.23	1.20	1.30	1.18	1.22
O/C ratio	0.73	0.68	0.67	0.65	0.69	0.67	0.49	0.35	0.47	0.33	0.46	0.33
DBE	8.93	8.9	8.75	8.62	8.47	8.58	9.05	9.7	8.85	9.07	9.05	9.78
AI_{mod}	0.04	0.04	0.04	0.01	0.05	0.02	0.22	0.24	0.23	0.21	0.24	0.23
Aromatics %	0.9	0.8	0.7	0.5	1.6	1.3	3	1.6	3	1.6	2.6	1.8

FT-ICR-MS is not a quantitative approach, and therefore no conclusions regarding concentrations along the flow path can be made with these data.

However, a decrease in the DOC concentration along the flow path was observed in not only this study but also Westphal et al. (2019) and could be indicative of microbial degradation. This is especially possible since a variety of microorganisms were detected in this study. The detection of Firmicutes, Proteobacteria, and *Thermotogae* under the extreme environmental conditions at the three sampling points is not unlikely. Firmicutes are known to form endospores (Cano and Borucki, 1995; Nicholson et al., 2002), which are highly resistant structures known to withstand conditions such as those in the power plant. Members of the Firmicutes (Filippidou et al., 2016) and Proteobacteria (Dib et al., 2008) have been detected in several extreme environments, showing their potential to withstand environmental conditions in deep geothermal reservoirs. Members of the phylum *Thermotogae* can be mesophilic, thermophilic, or hyperthermophilic, and most of the cultivated representatives have been obtained from extreme environments (Bhandari and Gupta, 2014).

In addition to *Bacillus*, some *Pseudomonas*, *Desulfotomaculum*, *Planktothrix*, and ASVs related to the BRH-c8a clade were also detected in the production side sample. Species of *Bacillus* spp. are capable of forming highly resistant endospores (Nicholson et al., 2000). Therefore, the dominance of *Bacillus* at the production side, with the highest fluid temperatures, is not surprising. A previous bacterial diversity study performed in Bad Blumau (Westphal et al., 2019) already reported the detection of members of the genus *Desulfotomaculum*. Furthermore, this genus has been detected in other geothermal systems, such as different terrestrial hot springs (Amin et al., 2013; Poratti et al., 2016), or in geothermal groundwater (Daumas et al., 1988). Therefore, it is also not surprising to find sequences (BRH-c8a clade) closely related to *Desulfotomaculum* (Sousa et al., 2018) in a geothermal system. Additionally, representatives of the genus *Pseudomonas* have been reported in the oxic zone of a geothermal system (Burté et al., 2019). The presence of

Cyanobacteria belonging to the genus *Planktothrix* is more surprising. Cyanobacteria are known for their phototrophic metabolism and would need at least occasional light exposure for active growth (Puente-Sánchez et al., 2018). However, Cyanobacteria have recently been found in different environments that are not exposed to light, such as the deep subsurface or close to hydrothermal vents (Hubalek et al., 2016; Puente-Sánchez et al., 2018; Chen et al., 2022). Moreover, Cyanobacteria are commonly found in geothermal environments (Ward et al., 2012). This indicates that the presence of Cyanobacteria in different ecosystems, such as the deep geothermal system, is possible.

The dominant genera in the heat central corresponded to *Caulobacter*, *Desulfotomaculum* (also detected on the production and injection sides), *Sphingobium*, SCADC1-2-3, and *Microbacterium*. Members of the genus *Caulobacter* and *Sphingobium* were detected in the oxic and anoxic zone, respectively, of the same geothermal system in which *Pseudomonas* was reported (Burté et al., 2019). The SCADC1-2-3 is a group of uncultured organisms that belongs to the *Desulfisporaceae* family (Gavrilov et al., 2022). The SCADC1-2-3 group is part of a family of thermophilic sulfate-reducing bacteria and has been detected in subsurface waters (Gavrilov et al., 2022). The *Microbacterium* species described so far are known to be tolerant to extreme conditions, for instance, to the presence of arsenic (Achour-Rokbani et al., 2010), and have been isolated notably from a heated aquifer bore well (Adelskov and Patel, 2017), surface hot springs (Mehetre et al., 2019), and from the Atacama Desert (Mandakovic et al., 2020).

In addition to *Desulfotomaculum*, which was highly dominant in the injection well, *Fervidobacterium*, *Pseudotherrmotoga*, and *Thermanaeromonas* and *Thermodesulfovibrio* with a low relative abundance were detected. The described species belonging to the genus *Fervidobacterium* are all anaerobic and extremely thermophilic, fermenting glucose to acetate and reducing sulfur to H_2S (Huber and Stetter, 2015). *Pseudotherrmotoga* are known thermophilic and anaerobic bacteria, isolated from hot springs and oil reservoirs (Farrell et al., 2021). *Thermanaeromonas* species are thermophilic

anaerobes that are capable of forming spores (Mori and Hanada, 2015). They were notably isolated from a geothermal aquifer (Mori et al., 2002) and a subterranean clay environment (Gam et al., 2016). *Thermodesulfovibrio* are also anaerobic thermophilic organisms that are able to oxidize organic substrates to acetate (Maki, 2015) and have been isolated from hydrothermal vent waters (Henry et al., 1994) or hot springs (Sonne-Hansen and Ahring, 1999).

The results of our study are largely consistent with those of a previous study investigating bacterial diversity in the fluids collected in 2011 and 2013 at Bad Blumau (Westphal et al., 2019). In that study, samples were also taken from the production well and the injection well. The third sampling point was located after CO₂ extraction, before the heat central. In our case, the third sampling point was located in the heat central itself. However, some differences were detected. In Westphal et al. (2019), the alpha-proteobacteria and beta-proteobacteria classes were found in the production fluids. In this study, alpha-proteobacteria were detected in the production fluids and after the heat central, but no beta-proteobacteria were detected as part of the most abundant classes (data not shown). Clostridia were detected in all fluids by Westphal et al. (2019), which was also the case here. The classes Actinobacteria, Clostridia, and Thermotogae were the dominant ones detected in the injection well by Westphal et al. (2019). The Clostridia class was detected in the different samples in both studies, and the Clostridia and Thermotogae classes became dominant in the injection well, displacing Actinobacteria, which were only present in a low relative abundance. Our observations also confirm the presence of the Bacilli class as a dominant class on the production side. Previously, Ignavibacteria and the Nitrospira class were detected in the injection fluids, but in our case, Ignavibacteria were detected in a very low abundance in the fluids from the heat central and the injection well, and Nitrospira was not detected. However, the class Thermodesulfovibrionia was detected in low abundance at the heat central and in the injection fluids and was previously part of the Nitrospira class (Rabus et al., 2015; Umezawa et al., 2021). Therefore, the difference in the Nitrospira class in our analysis compared to Westphal et al. (2019) may only reflect a change in the bacterial taxonomy. The genus *Desulfotomaculum* was consistently detected in the production well after CO₂ removal and in the injection well in both studies. In the production well, both Westphal et al. (2019) and the present study detected the class Bacilli and the genus *Pseudomonas*. Several genera, such as *Comamonas* and *Ralstonia*, were detected in the production fluids by Westphal et al. (2019) but were not among the top five genera observed in our study. Westphal et al. (2019) also detected *Thermodesulfovibrio*, *Desulfovirgula*, *Desulfovibrio*, *Fervidobacterium*, and *Thermanaeromonas* at the injection well. In our case, *Thermodesulfovibrio*, the *Fervidobacterium*, and *Thermanaeromonas* genera were also detected. One difference between the two studies lies in the detection of Cyanobacteria (*Planktothrix*) and *Planctomycetes* at the

production well, but none of these phyla were dominant. Overall, both studies highlight the changes in bacterial communities along the flow path, from the production to the injection well. Such differences in communities highlight the impact of fluid conditions on bacterial communities, with some bacteria replacing others as conditions change within the system (Alawi et al., 2011; Lerm et al., 2013; Westphal et al., 2019). Furthermore, this is consistent with tests to change bacterial communities by adding nitrate to the fluids, which led to changes in the community. More importantly, the consistency between two independent studies demonstrates that the communities have been relatively stable over several years. Differences in results may be due to differences in detection methods or small changes in the community. However, the dominant genera were the same as those detected previously, and the changes in the communities from production to injection well followed the same patterns as observed by Westphal et al. (2019). This confirms that the presence of these microorganisms in the Bad Blumau system was not only temporary, as a byproduct of maintenance work, for instance. Furthermore, despite a relatively high flow rate, changes in the microbial community show that these conditions are compatible with the reactivation and development of a microbial community.

Answering the second question posed for the discussion, (a) the decrease in DOC content in our March 2021 samples is likely due to microbial degradation and (b) the composition of the microbial community along the flow path is mainly driven by the given fluid temperature at the sampling points.

4.3 The role and origin of acetate: link to the active microbial community

Acetate forms the dominant part of the DOC in the fluid samples. Two possible sources for its presence in our samples were considered: abiotic (e.g., water–oil contact or inhibitor derived) and biotic as a byproduct of active microbial communities. The contact of water and oil is a known source of organic acid anions in the fluid and was suggested to increase the LMWA content due to the release of hydrophilic acids (Reinsel et al., 1994). Oil-field waters are generally described as containing predominantly acetate, but there were also detectable amounts of formate, propionate, butyrate, and valerate (Carothers and Kharaka, 1978; Hatton and Hanor, 1984; Kharaka et al., 1985, 1997). The organic acid anion content is less likely to be associated with the water–oil contact in our samples due to the lack of butyrate and valerate and only sporadic detection of propionate. However, consumption by microorganisms could be another reason for the absence of these organic acids. Thermodynamic conditions were found to be favorable for the abiotic generation of formate and acetate in deep fracture waters (Sherwood Lollar et al., 2021). However, the temperatures (25 °C) were significantly different from those in Bad Blumau. Abiotic acetate production has also been shown to

occur at a temperature of 60 °C at 2 bar and in the presence of a greigite (Fe_3S_4) catalyst (Preiner et al., 2020). However, abiotic production of acetate due to water–rock reactions appears to be correlated with the presence of formate (Kieft et al., 2018; Sherwood Lollar et al., 2021; McDermott et al., 2015; Lang et al., 2010), which is absent in the Bad Blumau samples. It is unlikely that abiotic reactions have a significant effect on the production of the acetate in Bad Blumau since no formate was detected.

Acetate is therefore most likely biogenic and might be formed as a primary breakdown product of complex organic matter due to the bacterial degradation by fermentative anaerobes. Metabolic pathways were predicted in our study using PICRUSt2 (Douglas et al., 2020) based on the composition of the microbial community. These predictions do not necessarily prove the existence of a given metabolism but can be a useful aid to guide future enrichment or the selective detection of specific microbial groups/metabolic processes. As acetate was present in Bad Blumau in large amounts (14.2–18.2 mg L⁻¹), all pathways related to acetate were evaluated (Fig. 6). Many microorganisms have the potential to use or produce acetate. This was also the case within the Bad Blumau fluid systems, where the production and use of acetate by microorganisms would be possible in the production well, the heat central, and the injection well.

Relatives of fermentative bacteria (*Thermoanaerobacter brockii*) were detected in the produced fluids by Westphal et al. (2019), which are described as producing lactic acid, acetic acid, H₂, and CO₂ as fermentation products. Macromolecular components of the scaling inhibitor are likely to act as an energy source and a carbon source for this fermentation process, as already suggested by Westphal et al. (2019). Some studies suggest that propionate and even butyrate may also be produced by the fermentation of organic matter (Sørensen et al., 1981; Lovley and Klug, 1986; Lovley and Phillips, 1989). The sporadic detection of propionate in the samples could be indicative of this process. The degradation products can be used as substrates by other microbial communities. Cross-feeding interactions were described, including sulfate-reducing bacteria using lactate for sulfate reduction and in turn providing hydrogen for hydrogenotrophic bacteria in the Bad Blumau fluids, leading to the formation of acetate as a degradation product. A gradual decrease in sulfate was observed only in samples from June 2021, which could be related to sulfate reduction in the power plant (Westphal et al., 2019). However, it is more likely that these concentrations represent the natural variability in the fluids, as the high fluid flow provides a continuous supply of sulfate.

Answering the third question posed for the discussion, water–oil contact and an abiotic origin can likely be excluded due to the absence of other LMWAs, while the inhibitor only induces a minimal amount of acetate (2.2 µg CL⁻¹). In conclusion, a microbial origin of the acetate as a result of fermentative processes is likely to account for the majority of the acetate present in our fluid samples.

5 Conclusions

With regard to the objectives of this study, it has been shown that various methods were successfully used to characterize DOM to provide a detailed description of the DOM present in the fluids. It was shown with LC-OCD and IC that the DOC consists predominantly of LMWAs. We successfully distinguished between natural and synthetic organic matter, revealing that the macromolecular DOM primarily consisted of O_x and S₁O_x compounds, which were predominantly derived from the synthetic scaling inhibitor. DOM compounds that were found in the inhibitor but not in the fluids, such as N₁O_x and N₁S₁O_x, might be absent due to (a) alteration by chemical reactions with the fluid, forming complexes; (b) degradation after injection into the fluids; (c) no detection in the fluid samples due to strong dilution of the inhibitor; or (d) degradation by microorganisms that target these specific compounds. With respect to objective 3, it can be concluded that the acetate present in the fluids is likely of biogenic origin as a product of fermentative bacteria, turning lysine, pyruvate, or hexitol into acetate. The dominant genera involved in these processes were *Bacillus* and *Desulfotomaculum*. Last but not least, with a view to objective 4, it can be stated that the concentrations of both DOC and the microbial communities change along the flow path. The change in DOC content is probably caused by microbial degradation. However, in terms of DOM composition, no specific change was observed along the flow path, and it does not correlate with changes in microbial diversity.

Additional insight with regard to chemical fluid composition, processes that occur along the flow path, and the origin of the dissolved organic matter was gained in the Bad Blumau geothermal power plant by evaluating organic compounds and the microbial community composition in the fluids. Both are rather complex. So far, no indications have been found that they contribute to changes in well productivity or injectivity. However, on a longer timescale the impact of the organic compounds can still be relevant, e.g., when decomposition processes are not possible in the inhibitor-enriched fluids. Overall, this information significantly adds to the understanding of fluid processes at a geothermal site and could be helpful in minimizing operational damage, such as biofilm formation and/or microbially induced corrosion.

Data availability. Microbial data: a bigger dataset, available as a Sequence Read Archive (SRA) under the accession number SUB13065233 on NCBI, contains the Illumina MiSeq sequences used within this study.

Organic and inorganic anion data, as well as DOC and bulk fraction data used in this study, can be accessed through <https://doi.org/10.5880/GFZ.4.8.2023.005> (Leins et al., 2023).

Supplement. The supplement related to this article is available online at: <https://doi.org/10.5194/bg-21-5457-2024-supplement>.

Author contributions. AVH, PJ, and SR designed the project. FE and DB took the samples. AL analyzed the organic compound data. DB analyzed the microbial data. GC performed the modeling of the metabolic capabilities of the present microorganisms. AL prepared and wrote the major part of the original draft with contributions from DB. AVH, FE, SP, PJ, and SR reviewed and edited the paper. All authors read and approved the final paper.

Competing interests. The contact author has declared that none of the authors has any competing interests.

Disclaimer. Publisher's note: Copernicus Publications remains neutral with regard to jurisdictional claims made in the text, published maps, institutional affiliations, or any other geographical representation in this paper. While Copernicus Publications makes every effort to include appropriate place names, the final responsibility lies with the authors.

Acknowledgements. We acknowledge the contributions of Kristin Günther and Cornelia Karger (both GFZ) for sample preparation and analyses of the organic compound, and Spa Therme Blumau Betriebs GmbH for providing the fluid samples.

Financial support. This research has been supported by the European Union's Horizon 2020 program (grant no. 850626) and the "Open Access Publikationskosten" Deutsche Forschungsgemeinschaft (DFG, German Research Foundation) – project number 491075472.

The article processing charges for this open-access publication were covered by the Helmholtz Centre Potsdam – GFZ German Research Centre for Geosciences.

Review statement. This paper was edited by Jack Middelburg and reviewed by two anonymous referees.

References

- Achour-Rokbani, A., Cordi, A., Poupin, P., Bauda, P., and Billard, P.: Characterization of the *ars* Gene Cluster from Extremely Arsenic-Resistant *Microbacterium* sp. Strain A33, *Appl. Environ. Microbiol.*, 76, 948–955, <https://doi.org/10.1128/AEM.01738-09>, 2010.
- Adelskov, J. and Patel, B. K. C.: Draft Genome Sequence of *Microbacterium* sp. TNHR37B Isolated from a Heated Aquifer Bore Well of the Great Artesian Basin, Australia, *Genome Announcements*, 5, e00251-17, <https://doi.org/10.1128/genomeA.00251-17>, 2017.
- Alawi, M., Lerm, S., Vetter, A., Wolfgramm, M., Seibt, A., and Würdemann, H.: Diversity of sulfate-reducing bacteria in a plant using deep geothermal energy, *Grundwasser*, 16, 105–112, <https://doi.org/10.1007/s00767-011-0164-y>, 2011.
- Alt-Epping, P., Waber, H., Diamond, L., and Eichinger, L.: Reactive transport modeling of the geothermal system at Bad Blumau, Austria: Implications of the combined extraction of heat and CO₂, *Geothermics*, 45, 18–30, <https://doi.org/10.1016/j.geothermics.2012.08.002>, 2013.
- Amin, O., Fardeau, M.-L., Valette, O., Hirschler-Réa, A., Barbe, V., Médigue, C., Vacherie, B., Ollivier, B., Bertin, P. N., and Dolla, A.: Genome Sequence of the Sulfate-Reducing Bacterium *Desulfotomaculum hydrothermale* Lam5^T, *Genome Announcements*, 1, e00114-12, <https://doi.org/10.1128/genomeA.00114-12>, 2013.
- Bae, E., Yeo, I. J., Jeong, B., Shin, Y., Shin, K.-H., and Kim, S.: Study of Double Bond Equivalents and the Numbers of Carbon and Oxygen Atom Distribution of Dissolved Organic Matter with Negative-Mode FT-ICR MS, *Anal. Chem.*, 83, 4193–4199, <https://doi.org/10.1021/ac200464q>, 2011.
- Bhandari, V. and Gupta, R. S.: The Phylum Thermotogae, in: *The Prokaryotes: Other Major Lineages of Bacteria and The Archaea*, edited by Rosenberg, E., DeLong, E. F., Lory, S., Stackebrandt, E., and Thompson, F., Springer Berlin Heidelberg, Berlin, Heidelberg, 989–1015, ISBN 978-3-642-38954-2, https://doi.org/10.1007/978-3-642-38954-2_118, 2014.
- Bolyen, E., Rideout, J. R., Dillon, M. R., Bokulich, N. A., Abnet, C. C., Al-Ghalith, G. A., Alexander, H., Alm, E. J., Arumugam, M., Asnicar, F., Bai, Y., Bisanz, J. E., Bittinger, K., Brejnrod, A., Brislawn, C. J., Brown, C. T., Callahan, B. J., Caraballo-Rodríguez, A. M., Chase, J., Cope, E. K., Da Silva, R., Diener, C., Dorrestein, P. C., Douglas, G. M., Durall, D. M., Duvallet, C., Edwardson, C. F., Ernst, M., Estaki, M., Fouquier, J., Gauglitz, J. M., Gibbons, S. M., Gibson, D. L., Gonzalez, A., Gorlick, K., Guo, J., Hillmann, B., Holmes, S., Holste, H., Huttenhower, C., Huttley, G. A., Janssen, S., Jarmusch, A. K., Jiang, L., Kaehler, B. D., Kang, K. B., Keefe, C. R., Keim, P., Kelley, S. T., Knights, D., Koester, I., Kosciulek, T., Kreps, J., Langille, M. G. I., Lee, J., Ley, R., Liu, Y.-X., Loftfield, E., Lozupone, C., Maher, M., Marotz, C., Martin, B. D., McDonald, D., McIver, L. J., Melnik, A. V., Metcalf, J. L., Morgan, S. C., Morton, J. T., Naimy, A. T., Navas-Molina, J. A., Nothias, L. F., Orchanian, S. B., Pearson, T., Peoples, S. L., Petras, D., Preuss, M. L., Pruesse, E., Rasmussen, L. B., Rivers, A., Robeson, M. S., Rosenthal, P., Segata, N., Shaffer, M., Shiffer, A., Sinha, R., Song, S. J., Spear, J. R., Swafford, A. D., Thompson, L. R., Torres, P. J., Trinh, P., Tripathi, A., Turnbaugh, P. J., Ul-Hasan, S., van der Hoof, J. J. J., Vargas, F., Vázquez-Baeza, Y., Vogtmann, E., von Hippel, M., Walters, W., Wan, Y., Wang, M., Warren, J., Weber, K. C., Williamson, C. H. D., Willis, A. D., Xu, Z. Z., Zaneveld, J. R., Zhang, Y., Zhu, Q., Knight, R., and Caporaso, J. G.: Reproducible, interactive, scalable and extensible microbiome data science using QIIME 2, *Nat. Biotechnol.*, 37, 852–857, <https://doi.org/10.1038/s41587-019-0209-9>, 2019.
- Brehme, M., Nowak, K., Abel, M., Siklosi, I., Willems, C., and Huenges, E.: Injection Triggered Occlusion of Flow Pathways in a Sedimentary Aquifer in Hungary, *World Geothermal Congress (WGC)*, 21–26 May 2020, Reykjavik, Iceland, <https://researchportal.hw.ac.uk/en/publications/>

- injection-triggered-occlusion-of-flow-pathways-in-a-sedimentary-a (last access: 1 December 2024), 2020.
- Burté, L., Cravotta, C. A. I., Bethencourt, L., Farasin, J., Pédrot, M., Dufresne, A., Gérard, M.-F., Baranger, C., Le Borgne, T., and Aquilina, L.: Kinetic Study on Clogging of a Geothermal Pumping Well Triggered by Mixing-Induced Biogeochemical Reactions, *Environ. Sci. Technol.*, 53, 5848–5857, <https://doi.org/10.1021/acs.est.9b00453>, 2019.
- Callahan, B. J., McMurdie, P. J., Rosen, M. J., Han, A. W., Johnson, A. J. A., and Holmes, S. P.: DADA2: High-resolution sample inference from Illumina amplicon data, *Nat. Method.*, 13, 581–583, <https://doi.org/10.1038/nmeth.3869>, 2016.
- Cano, R. J. and Borucki, M. K.: Revival and Identification of Bacterial Spores in 25- to 40-Million-Year-Old Dominican Amber, *Science*, 268, 1060–1064, <https://doi.org/10.1126/science.7538699>, 1995.
- Carothers, W. W. and Kharaka, Y. K.: Aliphatic Acid Anions in Oil-Field Waters—Implications for Origin of Natural Gas1, *AAPG Bull.*, 62, 2441–2453, <https://doi.org/10.1306/C1EA5521-16C9-11D7-8645000102C1865D>, 1978.
- Chen, H., Li, D. H., Jiang, A. J., Li, X. G., Wu, S. J., Chen, J. W., Qu, M. J., Qi, X. Q., Dai, J., Zhao, R., Zhang, W.-J., Liu, S. S., and Wu, L.-F.: Metagenomic analysis reveals wide distribution of phototrophic bacteria in hydrothermal vents on the ultraslow-spreading Southwest Indian Ridge, *Mar. Life Sci. Technol.*, 4, 255–267, <https://doi.org/10.1007/s42995-021-00121-y>, 2022.
- D’Andrilli, J., Dittmar, T., Koch, B. P., Purcell, J. M., Marshall, A. G., and Cooper, W. T.: Comprehensive characterization of marine dissolved organic matter by Fourier transform ion cyclotron resonance mass spectrometry with electrospray and atmospheric pressure photoionization, *Rapid Commun. Mass Sp.*, 24, 643–650, <https://doi.org/10.1002/rcm.4421>, 2010.
- Daumas, S., Cord-Ruwisch, R., and Garcia, J. L.: *Desulfotomaculum geothermicum* sp. nov., a thermophilic, fatty acid-degrading, sulfate-reducing bacterium isolated with H₂ from geothermal ground water, *Antonie van Leeuwenhoek*, 54, 165–178, <https://doi.org/10.1007/BF00419203>, 1988.
- De Leeuw, J. W. and Largeau, C.: A Review of Macromolecular Organic Compounds That Comprise Living Organisms and Their Role in Kerogen, Coal, and Petroleum Formation, Springer US, Boston, MA, 23–72, ISBN 978-1-4615-2890-6, https://doi.org/10.1007/978-1-4615-2890-6_2, 1993.
- Demir, M. M., Baba, A., Atilla, V., and İnanlı, M.: Types of the scaling in hyper saline geothermal system in northwest Turkey, *Geothermics*, 50, 1–9, <https://doi.org/10.1016/j.geothermics.2013.08.003>, 2014.
- Dib, J., Motok, J., Zenoff, V. F., Ordoñez, O., and Farías, M. E.: Occurrence of Resistance to Antibiotics, UV-B, and Arsenic in Bacteria Isolated from Extreme Environments in High-Altitude (Above 4400 m) Andean Wetlands, *Curr. Microbiol.*, 56, 510–517, <https://doi.org/10.1007/s00284-008-9103-2>, 2008.
- Dittmar, T., Koch, B., Hertkorn, N., and Kattner, G.: A simple and efficient method for the solid-phase extraction of dissolved organic matter (SPE-DOM) from seawater, *Limnol. Oceanogr.-Method.*, 6, 230–235, <https://doi.org/10.4319/lom.2008.6.230>, 2008.
- Douglas, G. M., Maffei, V. J., Zaneveld, J. R., Yurgel, S. N., Brown, J. R., Taylor, C. M., Huttenhower, C., and Langille, M. G. I.: PICRUSt2 for prediction of metagenome functions, *Nat. Biotechnol.*, 38, 685–688, <https://doi.org/10.1038/s41587-020-0548-6>, 2020.
- D’Andrilli, J., Chanton, J. P., Glaser, P. H., and Cooper, W. T.: Characterization of dissolved organic matter in northern peatland soil porewaters by ultra high resolution mass spectrometry, *Org. Geochem.*, 41, 791–799, <https://doi.org/10.1016/j.orggeochem.2010.05.009>, 2010.
- Farrell, A., Nesbø, C. L., Zhaxybayeva, O., and L’Haridon, S.: *Pseudothermotoga*, John Wiley and Sons Ltd, 1–12, ISBN 9781118960608, <https://doi.org/10.1002/9781118960608.gbm01861>, 2021.
- Filippidou, S., Wunderlin, T., Junier, T., Jeanneret, N., Dorador, C., Molina, V., Johnson, D. R., and Junier, P.: A Combination of Extreme Environmental Conditions Favor the Prevalence of Endospore-Forming Firmicutes, *Front. Microbiol.*, 7, 1707, <https://doi.org/10.3389/fmicb.2016.01707>, 2016.
- Fisher, J. and Boles, J.: Water–rock interaction in Tertiary sandstones, San Joaquin basin, California, U.S.A.: Diagenetic controls on water composition, *Chem. Geol.*, 82, 83–101, [https://doi.org/10.1016/0009-2541\(90\)90076-J](https://doi.org/10.1016/0009-2541(90)90076-J), 1990.
- Flatt, R. and Schober, I.: 7 – Superplasticizers and the rheology of concrete, in: *Understanding the Rheology of Concrete*, edited by Roussel, N., Woodhead Publishing Series in Civil and Structural Engineering, Woodhead Publishing, 144–208, ISBN 978-0-85709-028-7, <https://doi.org/10.1533/9780857095282.2.144>, 2012.
- Gam, Z. B. A., Dumas, S., Casalot, L., Bartoli-Joseph, M., Necib, S., Linard, Y., and Labat, M.: *Thermanaeromonas burensis* sp. nov., a thermophilic anaerobe isolated from a subterranean clay environment, *Int. J. System. Evol. Microbiol.*, 66, 445–449, <https://doi.org/10.1099/ijsem.0.000739>, 2016.
- Gavrilov, S. N., Potapov, E. G., Prokof’eva, M. I., Klyukina, A. A., Merkel, A. Y., Maslov, A. A., and Zavarzina, D. G.: Diversity of Novel Uncultured Prokaryotes in Microbial Communities of the Yessentukskoye Underground Mineral Water Deposit, *Microbiology*, 91, 28–44, <https://doi.org/10.1134/S0026261722010039>, 2022.
- Goldbrunner, J.: Hydrogeology of deep groundwaters in Austria, *Mitt. Österr. Geol. Ges.*, 92, 281–294, ISSN: 0251-7493, 2000.
- Goldbrunner, J.: State, possible future developments in and barriers to the exploration and exploitation of geothermal energy in Austria – country update, *Proceedings World Geothermal Congress (WGC)*, Antalya, Turkey, 24–29 April, <https://www.geothermal-energy.org/pdf/IGAstandard/WGC/2005/0147.pdf> (last access: 1 December 2024), 2005.
- Gomez-Saez, G. V., Niggemann, J., Dittmar, T., Pohlabein, A. M., Lang, S. Q., Noowong, A., Pichler, T., Wörmer, L., and Bühring, S. I.: Molecular evidence for abiotic sulfuration of dissolved organic matter in marine shallow hydrothermal systems, *Geochim. Cosmochim. Acta*, 190, 35–52, <https://doi.org/10.1016/j.gca.2016.06.027>, 2016.
- Hatton, R. and Hanor, J.: Dissolved volatile fatty acids in subsurface, hydropressure brines: a review of published literature on occurrence, genesis and thermodynamic properties, *Technical Report for Geopressured-Geothermal Activities in Louisiana: Final Geological Report for the Period 1 November 1981 to 31 October 1982*, DOE Report No. DOE/NV/10174-3, 1984.
- Hawkes, J. A., Hansen, C. T., Goldhammer, T., Bach, W., and Dittmar, T.: Molecular alteration of marine dis-

- solved organic matter under experimental hydrothermal conditions, *Geochim. Cosmochim. Acta*, 175, 68–85, <https://doi.org/10.1016/j.gca.2015.11.025>, 2016.
- Henry, E. A., Devereux, R., Maki, J. S., Gilmour, C. C., Woese, C. R., Mandelco, L., Schauder, R., Remsen, C. C., and Mitchell, R.: Characterization of a new thermophilic sulfate-reducing bacterium, *Arch. Microbiol.*, 161, 62–69, <https://doi.org/10.1007/BF00248894>, 1994.
- Herlemann, D. P., Labrenz, M., Jürgens, K., Bertilsson, S., Waniek, J. J., and Andersson, A. F.: Transitions in bacterial communities along the 2000 km salinity gradient of the Baltic Sea, *ISME J.*, 5, 1571–1579, <https://doi.org/10.1038/ismej.2011.41>, 2011.
- Hewlett, P. C., Justnes, H., and Edmeades, R. M.: 14 – Cement and Concrete Admixtures, in: *Lea's Chemistry of Cement and Concrete*, 5th Edn., edited by: Hewlett, P. C. and Liska, M., Butterworth-Heinemann, 5th Edn., 641–698, ISBN 978-0-08-100773-0, <https://doi.org/10.1016/B978-0-08-100773-0.00014-9>, 2019.
- Hubalek, V., Wu, X., Eiler, A., Buck, M., Heim, C., Dopson, M., Bertilsson, S., and Ionescu, D.: Connectivity to the surface determines diversity patterns in subsurface aquifers of the Fennoscandian shield, *ISME J.*, 10, 2447–2458, <https://doi.org/10.1038/ismej.2016.36>, 2016.
- Huber, R. and Stetter, K. O.: *Fervidobacterium*, John Wiley and Sons Ltd, 1–5, ISBN 9781118960608, <https://doi.org/10.1002/9781118960608.gbm01269>, 2015.
- Huber, S. A. and Frimmel, F. H.: Size-exclusion chromatography with organic carbon detection (LC-OCD): a fast and reliable method for the characterization of hydrophilic organic matter in natural waters, *Vom Wasser*, 86, 277–290, 1996.
- Huber, S. A., Balz, A., Abert, M., and Pronk, W.: Characterisation of aquatic humic and non-humic matter with size-exclusion chromatography – organic carbon detection – organic nitrogen detection (LC-OCD-OND), *Water Res.*, 45, 879–885, <https://doi.org/10.1016/j.watres.2010.09.023>, 2011.
- Hubmann, B., Suttner, T., and Messner, F.: Geologic frame of Palaeozoic reefs in Austria with special emphasis on Devonian reef-architecture of the Graz Palaeozoic, *Joanneum Geologie und Paläontologie*, 8, 47–72, 2006.
- Inagaki, F., Motomura, Y., and Ogata, S.: Microbial silica deposition in geothermal hot waters, *Appl. Microbiol. Biotechnol.*, 60, 605–611, <https://doi.org/10.1007/s00253-002-1100-y>, 2003.
- Kharaka, Y., Maest, A., Carothers, W., Law, L., Lamothe, P., and Fries, T.: Geochemistry of metal-rich brines from central Mississippi Salt Dome basin, USA, *Appl. Geochem.*, 2, 543–561, [https://doi.org/10.1016/0883-2927\(87\)90008-4](https://doi.org/10.1016/0883-2927(87)90008-4), 1987.
- Kharaka, Y. K., Law, L. M., Carothers, W. W., and Goerlitz, D. F.: Role of Organic Species Dissolved in Formation Waters from Sedimentary Basins in Mineral Diagenesis, in: *Roles of Organic Matter in Sediment Diagenesis*, ISBN electronic: 9781565761049, ISBN print: 0918985595, SEPM Soc. *Sediment. Geol.*, 38, <https://doi.org/10.2110/pec.86.38>, 1985.
- Kharaka, Y. K., Giordano, T. H., and Lundegard, P. D.: Distribution and Origin of Organic Ligands in Subsurface Waters from Sedimentary Basins, in: *Ore Genesis and Exploration: The Roles of Organic Matter*, *Soc. Econ. Geol.*, 9, 119–129, <https://doi.org/10.5382/Rev.09.06>, 1997.
- Kieft, T. L., Walters, C. C., Higgins, M. B., Mennito, A. S., Clewett, C. F., Heuer, V., Pullin, M. J., Hendrickson, S., van Heerden, E., Sherwood Lollar, B., Lau, M. C., and Onstott, T.: Dissolved organic matter compositions in 0.6–3.4 km deep fracture waters, Kaapvaal Craton, South Africa, *Org. Geochem.*, 118, 116–131, <https://doi.org/10.1016/j.orggeochem.2018.02.003>, 2018.
- Kim, S., Kramer, R. W., and Hatcher, P. G.: Graphical Method for Analysis of Ultrahigh-Resolution Broadband Mass Spectra of Natural Organic Matter, the Van Krevelen Diagram, *Anal. Chem.*, 75, 5336–5344, <https://doi.org/10.1021/ac034415p>, 2003.
- King, R., Bonfiglio, R., Fernandez-Metzler, C., Miller-Stein, C., and Olah, T.: Mechanistic investigation of ionization suppression in electrospray ionization, *J. Am. Soc. Mass Sp.*, 11, 942–950, [https://doi.org/10.1016/S1044-0305\(00\)00163-X](https://doi.org/10.1016/S1044-0305(00)00163-X), 2000.
- Koch, B. P. and Dittmar, T.: From mass to structure: an aromaticity index for high-resolution mass data of natural organic matter, *Rapid Commun. Mass Sp.*, 20, 926–932, <https://doi.org/10.1002/rcm.2386>, 2006.
- Koch, B. P., Ludwigowski, K.-U., Kattner, G., Dittmar, T., and Witt, M.: Advanced characterization of marine dissolved organic matter by combining reversed-phase liquid chromatography and FT-ICR-MS, *Mar. Chem.*, 111, 233–241, <https://doi.org/10.1016/j.marchem.2008.05.008>, 2008.
- Lang, S. Q., Butterfield, D. A., Schulte, M., Kelley, D. S., and Lilley, M. D.: Elevated concentrations of formate, acetate and dissolved organic carbon found at the Lost City hydrothermal field, *Geochim. Cosmochim. Acta*, 74, 941–952, <https://doi.org/10.1016/j.gca.2009.10.045>, 2010.
- Lang, S. Q., Früh-Green, G. L., Bernasconi, S. M., Brazelton, W. J., Schrenk, M. O., and McGonigle, J. M.: Deeply-sourced formate fuels sulfate reducers but not methanogens at Lost City hydrothermal field, *Sci. Rep.*, 8, 755, <https://doi.org/10.1038/s41598-017-19002-5>, 2018.
- Leins, A., Bregnard, D., Vieth-Hillebrand, A., Junier, P., and Regenspurg, S.: Dissolved organic compounds in geothermal fluids used for energy production: a review, *Geotherm. Energ.*, 10, 9, <https://doi.org/10.1186/s40517-022-00220-8>, 2022.
- Leins, A., Vieth-Hillebrand, A., Günther, K., and Regenspurg, S.: Dissolved organic compounds in geothermal fluids used for energy production – part II, GFZ Data Services [data set], <https://doi.org/10.5880/GFZ.4.8.2023.005>, 2023.
- Lerm, S., Westphal, A., Miethling-Graff, R., Alawi, M., Seibt, A., Wolfgramm, M., and Würdemann, H.: Thermal effects on microbial composition and microbiologically induced corrosion and mineral precipitation affecting operation of a geothermal plant in a deep saline aquifer, *Extremophiles*, 17, 311–327, <https://doi.org/10.1007/s00792-013-0518-8>, 2013.
- Little, B. J. and Lee, J. S.: *Microbiologically Influenced Corrosion*, Chap. 27, John Wiley and Sons Ltd, ISBN 9781119019213, 387–398, <https://doi.org/10.1002/9781119019213.ch27>, 2015.
- Longnecker, K., Sievert, S. M., Sylva, S. P., Seewald, J. S., and Kujawinski, E. B.: Dissolved organic carbon compounds in deep-sea hydrothermal vent fluids from the East Pacific Rise at 9°50' N, *Org. Geochem.*, 125, 41–49, <https://doi.org/10.1016/j.orggeochem.2018.08.004>, 2018.
- Lovley, D. R. and Klug, M. J.: Model for the distribution of sulfate reduction and methanogenesis in freshwater sediments, *Geochim. Cosmochim. Acta*, 50, 11–18, [https://doi.org/10.1016/0016-7037\(86\)90043-8](https://doi.org/10.1016/0016-7037(86)90043-8), 1986.

- Lovley, D. R. and Phillips, E. J. P.: Requirement for a Microbial Consortium To Completely Oxidize Glucose in Fe(III)-Reducing Sediments, *Appl. Environ. Microbiol.*, 55, 3234–3236, <https://doi.org/10.1128/aem.55.12.3234-3236.1989>, 1989.
- Madirisha, M., Hack, R., and van der Meer, F.: Simulated microbial corrosion in oil, gas and non-volcanic geothermal energy installations: The role of biofilm on pipeline corrosion, *Energ. Rep.*, 8, 2964–2975, <https://doi.org/10.1016/j.egy.2022.01.221>, 2022.
- Maki, J. S.: *Thermodesulfovibrio*, John Wiley and Sons Ltd, 1–9, ISBN 9781118960608, <https://doi.org/10.1002/9781118960608.gbm00781>, 2015.
- Mandakovic, D., Cintolesi, A., Maldonado, J., Mendoza, S. N., Aite, M., Gaete, A., Saitua, F., Allende, M., Cambiazo, V., Siegel, A., Maas, A., González, M., and Latorre, M.: Genome-scale metabolic models of Microbacterium species isolated from a high altitude desert environment, *Sci. Rep.*, 10, 1–13, <https://doi.org/10.1038/s41598-020-62130-8>, 2020.
- McDermott, J. M., Seewald, J. S., German, C. R., and Sylva, S. P.: Pathways for abiotic organic synthesis at submarine hydrothermal fields, *P. Natl. Acad. Sci. USA*, 112, 7668–7672, <https://doi.org/10.1073/pnas.1506295112>, 2015.
- McDonough, L. K., Rutledge, H., O'Carroll, D. M., Andersen, M. S., Meredith, K., Behnke, M. I., Spencer, R. G., McKenna, A. M., Marjo, C. E., Oudone, P., and Baker, A.: Characterisation of shallow groundwater dissolved organic matter in aeolian, alluvial and fractured rock aquifers, *Geochim. Cosmochim. Acta*, 273, 163–176, <https://doi.org/10.1016/j.gca.2020.01.022>, 2020.
- McDonough, L. K., Andersen, M. S., Behnke, M. I., Rutledge, H., Oudone, P., Meredith, K., O'Carroll, D. M., Santos, I. R., Marjo, C. E., Spencer, R. G. M., McKenna, A. M., and Baker, A.: A new conceptual framework for the transformation of groundwater dissolved organic matter, *Nat. Commun.*, 13, 2153, <https://doi.org/10.1038/s41467-022-29711-9>, 2022.
- McMurdie, P. and Paulson, J.: biomformat: An interface package for the BIOM file format, R/Bioconductor Package, version 1.0, 2016.
- Mehetre, G. T., J. S., V., Burkul, B. B., Desai, D., B., S., Dharme, M. S., and Dastager, S. G.: Bioactivities and molecular networking-based elucidation of metabolites of potent actinobacterial strains isolated from the Unkeshwar geothermal springs in India, *RSC Adv.*, 9, 9850–9859, <https://doi.org/10.1039/C8RA09449G>, 2019.
- Minor, E. C., Steinbring, C. J., Longnecker, K., and Kujawinski, E. B.: Characterization of dissolved organic matter in Lake Superior and its watershed using ultrahigh resolution mass spectrometry, *Org. Geochem.*, 43, 1–11, <https://doi.org/10.1016/j.orggeochem.2011.11.007>, 2012.
- Mori, K. and Hanada, S.: *Thermanaeromonas*, John Wiley and Sons Ltd, 1–5, ISBN 9781118960608, <https://doi.org/10.1002/9781118960608.gbm00750>, 2015.
- Mori, K., Hanada, S., Maruyama, A., and Marumo, K.: *Thermanaeromonas toyohensis* gen. nov., sp. nov., a novel thermophilic anaerobe isolated from a subterranean vein in the Toyoha Mines, *Int. J. Syst. Evol. Micr.*, 52, 1675–1680, <https://doi.org/10.1099/00207713-52-5-1675>, 2002.
- Nicholson, W. L., Munakata, N., Horneck, G., Melosh, H. J., and Setlow, P.: Resistance of *Bacillus* Endospores to Extreme Terrestrial and Extraterrestrial Environments, *Microbiol. Mol. Biol. Rev.*, 64, 548–572, <https://doi.org/10.1128/MMBR.64.3.548-572.2000>, 2000.
- Nicholson, W. L., Fajardo-Cavazos, P., Rebeil, R., Slieman, T. A., Riesenman, P. J., Law, J. F., and Xue, Y.: Bacterial endospores and their significance in stress resistance, *Antonie van Leeuwenhoek*, 81, 27–32, <https://doi.org/10.1023/A:1020561122764>, 2002.
- Noowong, A., Gomez-Saez, G. V., Hansen, C. T., Schwarz-Schampera, U., Koschinsky, A., and Dittmar, T.: Imprint of Kairei and Pelagia deep-sea hydrothermal systems (Indian Ocean) on marine dissolved organic matter, *Org. Geochem.*, 152, 104141, <https://doi.org/10.1016/j.orggeochem.2020.104141>, 2021.
- Oksanen, J., Simpson, G. L., Blanchet, F. G., Kindt, R., Legendre, P., Minchin, P. R., O'Hara, R., Solyomos, P., Stevens, M. H. H., Szoecs, E., Wagner, H., Barbour, M., Bedward, M., Bolker, B., Borcard, D., Carvalho, G., Chirico, M., De Caceres, M., Durand, S., Evangelista, H. B. A., FitzJohn, R., Friendly, M., Furneaux, B., Hannigan, G., Hill, M. O., Lahti, L., McGlinn, D., Ouellette, M.-H., Ribeiro Cunha, E., Smith, T., Stier, A., Ter Braak, C. J., and Weedon, J.: vegan: Community Ecology Package [code], <https://CRAN.R-project.org/package=vegan> (last access: 2 September 2022), 2022.
- Penru, Y., Simon, F. X., Guastalli, A. R., Esplugas, S., Llorens, J., and Baig, S.: Characterization of natural organic matter from Mediterranean coastal seawater, *J. Water Suppl. Res. T.*, 62, 42–51, <https://doi.org/10.2166/aqua.2013.113>, 2013.
- Poratti, G. W., Yaakop, A. S., Chan, C. S., Urbietta, M. S., Chan, K.-G., Ee, R., Tan-Guan-Sheng, A., Goh, K. M., and Donati, E. R.: Draft Genome Sequence of the Sulfate-Reducing Bacterium *Desulfotomaculum copahuensis* Strain CINDEFI1 Isolated from the Geothermal Copahue System, Neuquén, Argentina, *Genome Announcements*, 4, e00870-16, <https://doi.org/10.1128/genomeA.00870-16>, 2016.
- Preiner, M., Igarashi, K., Muchowska, K. B., Yu, M., Varma, S. J., Kleineremanns, K., Nobu, M. K., Kamagata, Y., Tüysüz, H., Moran, J., and Martin, W. F.: A hydrogen-dependent geochemical analogue of primordial carbon and energy metabolism, *Nat. Ecol. Evol.*, 4, 534–542, <https://doi.org/10.1038/s41559-020-1125-6>, 2020.
- Puente-Sánchez, F., Arce-Rodríguez, A., Oggerin, M., García-Villadangos, M., Moreno-Paz, M., Blanco, Y., Rodríguez, N., Bird, L., Lincoln, S. A., Tornos, F., Prieto-Ballesteros, O., Freeman, K. H., Pieper, D. H., Timmis, K. N., Amils, R., and Parro, V.: Viable cyanobacteria in the deep continental subsurface, *P. Natl. Acad. Sci. USA*, 115, 10702–10707, <https://doi.org/10.1073/pnas.1808176115>, 2018.
- Quast, C., Pruesse, E., Yilmaz, P., Gerken, J., Schweer, T., Yarza, P., Peplies, J., and Glöckner, F. O.: The SILVA ribosomal RNA gene database project: improved data processing and web-based tools, *Nucl. Acid. Res.*, 41, D590–D596, <https://doi.org/10.1093/nar/gks1219>, 2012.
- R Core Team: R: A Language and Environment for Statistical Computing, R Foundation for Statistical Computing [code], Vienna, Austria, <https://www.R-project.org/> (last access: 2 September 2022), 2020.
- Rabus, R., Venceslau, S. S., Wöhlbrand, L., Voordouw, G., Wall, J. D., and Pereira, I. A. C.: Chapter Two – A Post-Genomic View of the Ecophysiology, Catabolism and Biotechnological Rele-

- vance of Sulphate-Reducing Prokaryotes, *Adv. Microb. Physiol.*, 66, 55–321, <https://doi.org/10.1016/bs.ampbs.2015.05.002>, 2015.
- Regenspurg, S., Feldbusch, E., Norden, B., and Tichomirowa, M.: Fluid-rock interactions in a geothermal Rotliegend/Permo-Carboniferous reservoir (North German Basin), *Appl. Geochem.*, 69, 12–27, <https://doi.org/10.1016/j.apgeochem.2016.03.010>, 2016.
- Reinsel, M. A., Borkowski, J. J., and Sears, J. T.: Partition coefficients for acetic, propionic, and butyric acids in a crude oil/water system, *J. Chem. Eng. Data*, 39, 513–516, <https://doi.org/10.1021/je00015a026>, 1994.
- Rognes, T., Flouri, T., Nichols, B., Quince, C., and Mahé, F.: VSEARCH: a versatile open source tool for metagenomics, *PeerJ*, 4, e2584, <https://doi.org/10.7717/peerj.2584>, 2016.
- Rossel, P. E., Bienhold, C., Boetius, A., and Dittmar, T.: Dissolved organic matter in pore water of Arctic Ocean sediments: Environmental influence on molecular composition, *Org. Geochem.*, 97, 41–52, <https://doi.org/10.1016/j.orggeochem.2016.04.003>, 2016.
- Rossel, P. E., Stubbins, A., Rebling, T., Koschinsky, A., Hawkes, J. A., and Dittmar, T.: Thermally altered marine dissolved organic matter in hydrothermal fluids, *Org. Geochem.*, 110, 73–86, <https://doi.org/10.1016/j.orggeochem.2017.05.003>, 2017.
- Schmidt, F., Elvert, M., Koch, B. P., Witt, M., and Hinrichs, K.-U.: Molecular characterization of dissolved organic matter in pore water of continental shelf sediments, *Geochim. Cosmochim. Acta*, 73, 3337–3358, <https://doi.org/10.1016/j.gca.2009.03.008>, 2009.
- Sherwood Lollar, B., Heuer, V., McDermott, J., Tille, S., Warr, O., Moran, J., Telling, J., and Hinrichs, K.-U.: A window into the abiotic carbon cycle – Acetate and formate in fracture waters in 2.7 billion year-old host rocks of the Canadian Shield, *Geochim. Cosmochim. Acta*, 294, 295–314, <https://doi.org/10.1016/j.gca.2020.11.026>, 2021.
- Sleighter, R. L. and Hatcher, P. G.: The application of electrospray ionization coupled to ultrahigh resolution mass spectrometry for the molecular characterization of natural organic matter, *J. Mass Spectrom.*, 42, 559–574, <https://doi.org/10.1002/jms.1221>, 2007.
- Sleighter, R. L. and Hatcher, P. G.: Molecular characterization of dissolved organic matter (DOM) along a river to ocean transect of the lower Chesapeake Bay by ultrahigh resolution electrospray ionization Fourier transform ion cyclotron resonance mass spectrometry, *Mar. Chem.*, 110, 140–152, <https://doi.org/10.1016/j.marchem.2008.04.008>, 2008.
- Sonne-Hansen, J. and Ahring, B. K.: *Thermodesulfobacterium hveragerdense* sp.nov., and *Thermodesulfobacterium islandicus* sp.nov., Two Thermophilic Sulfate Reducing Bacteria Isolated from a Icelandic Hot Spring, *System. Appl. Microbiol.*, 22, 559–564, [https://doi.org/10.1016/S0723-2020\(99\)80009-5](https://doi.org/10.1016/S0723-2020(99)80009-5), 1999.
- Sørensen, J., Christensen, D., and Jørgensen, B. B.: Volatile Fatty Acids and Hydrogen as Substrates for Sulfate-Reducing Bacteria in Anaerobic Marine Sediment, *Appl. Environ. Microbiol.*, 42, 5–11, <https://doi.org/10.1128/aem.42.1.5-11.1981>, 1981.
- Sousa, D. Z., Visser, M., van Gelder, A. H., Boeren, S., Pieterse, M. M., Pinkse, M. W. H., Verhaert, P. D. E. M., Vogt, C., Franke, S., Kümmel, S., and Stams, A. J. M.: The deep-subsurface sulfate reducer *Desulfotomaculum kuznetsovii* employs two methanol-degrading pathways, *Nat. Commun.*, 9, 239, <https://doi.org/10.1038/s41467-017-02518-9>, 2018.
- Umezawa, K., Kojima, H., Kato, Y., and Fukui, M.: *Dissulfurispira thermophila* gen. nov., sp. nov., a thermophilic chemolithoautotroph growing by sulfur disproportionation, and proposal of novel taxa in the phylum Nitrospirota to reclassify the genus *Thermodesulfobacterium*, *System. Appl. Microbiol.*, 44, 126184, <https://doi.org/10.1016/j.syapm.2021.126184>, 2021.
- Vetter, A.: The influence of geothermal plants on the biogeochemistry of the microbial ecosystems in aquifers, Doctoral thesis, Technische Universität Berlin, Fakultät VI – Planen Bauen Umwelt, Berlin, <https://doi.org/10.14279/depositonce-3419>, 2012.
- Ward, D. M., Castenholz, R. W., and Miller, S. R.: Cyanobacteria in Geothermal Habitats, in: *Ecology of Cyanobacteria II: Their Diversity in Space and Time*, edited by: Whitton, B. A., Springer Netherlands, Dordrecht, 39–63, ISBN 978-94-007-3855-3, https://doi.org/10.1007/978-94-007-3855-3_3, 2012.
- Westphal, A., Eichinger, F., Eichinger, L., and Würdemann, H.: Change in the microbial community of saline geothermal fluids amended with a scaling inhibitor: effects of heat extraction and nitrate dosage, *Extremophiles*, 23, 283–304, <https://doi.org/10.1007/s00792-019-01080-0>, 2019.
- Wickham, H.: *ggplot2: Elegant Graphics for Data Analysis*, Springer-Verlag New York [code], ISBN 978-3-319-24277-4, <https://ggplot2.tidyverse.org> (last access: 2 September 2022), 2016.
- Wickham, H., Averick, M., Bryan, J., Chang, W., McGowan, L. D., François, R., Grolemund, G., Hayes, A., Henry, L., Hester, J., Kuhn, M., Pedersen, T. L., Miller, E., Bache, S. M., Müller, K., Ooms, J., Robinson, D., Seidel, D. P., Spinu, V., Takahashi, K., Vaughan, D., Wilke, C., Woo, K., and Yutani, H.: Welcome to the tidyverse, *J. Open Source Softw.*, 4, 1686, <https://doi.org/10.21105/joss.01686>, 2019.
- Wunderlin, T., Junier, T., Roussel-Delif, L., Jeanneret, N., and Junier, P.: Stage 0 sporulation gene A as a molecular marker to study diversity of endospore-forming Firmicutes, *Environ. Microbiol. Rep.*, 5, 911–924, <https://doi.org/10.1111/1758-2229.12094>, 2013.
- Zhu, Y., Vieth-Hillebrand, A., Wilke, F. D., and Horsfield, B.: Characterization of water-soluble organic compounds released from black shales and coals, *International J. Coal Geol.*, 150/151, 265–275, <https://doi.org/10.1016/j.coal.2015.09.009>, 2015.
- Zhu, Y., Vieth-Hillebrand, A., Noah, M., and Poetz, S.: Molecular characterization of extracted dissolved organic matter from New Zealand coals identified by ultrahigh resolution mass spectrometry, *Int. J. Coal Geol.*, 203, 74–86, <https://doi.org/10.1016/j.coal.2019.01.007>, 2019.